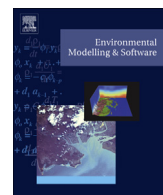




Contents lists available at ScienceDirect

## Environmental Modelling &amp; Software

journal homepage: [www.elsevier.com/locate/envsoft](http://www.elsevier.com/locate/envsoft)

## Stochastic reconstruction of paleovalley bedrock morphology from sparse datasets

J.C. Castilla-Rho <sup>a,c,d,\*</sup>, G. Mariethoz <sup>a,c,d</sup>, B.F.J. Kelly <sup>b,c,d</sup>, M.S. Andersen <sup>a,c,d</sup><sup>a</sup>School of Civil and Environmental Engineering, University of New South Wales, Sydney, NSW 2052, Australia<sup>b</sup>School Biological, Earth and Environmental Sciences, University of New South Wales, Sydney, NSW 2052, Australia<sup>c</sup>Connected Waters Initiative Research Centre, University of New South Wales, Sydney, NSW 2052, Australia<sup>d</sup>Affiliated with the National Centre for Groundwater Research and Training (NCGRT), Australia

## ARTICLE INFO

## Article history:

Received 19 March 2013

Received in revised form

25 August 2013

Accepted 29 October 2013

Available online 7 December 2013

## Keywords:

Geological uncertainty  
 Stochastic hydrogeology  
 Geological analog  
 Geostatistics  
 Spatial interpolation

## ABSTRACT

Stochastic groundwater models enable the characterization of geological uncertainty. Often the major source of uncertainty is not related to aquifer heterogeneity, but to the general shape of the aquifer. This is especially the case in paleovalley-type alluvial aquifers where the bedrock surface limits the extent of easily extractable groundwater. Determining the shape of a bedrock surface is not straightforward, because it is typically non-stationary and defined by few data points that are generally far apart. This paper presents a new workflow for the stochastic reconstruction of bedrock surfaces using limited datasets that are typically available for aquifer characterization. The method is based on a lateral propagation of basement cross-sections interpreted from geophysical surveys, and conditions the reconstructed surface to existing well-log data and digital elevation model. To alleviate the typical limitations of sparse data, we use an analog approach to incorporate prior geological knowledge. We test the methodology on a synthetic example and a dataset from an alluvial aquifer in Northern Chile. Results of these case studies show that the algorithm is capable of enforcing the general notion of structural continuity, with the aquifer shape being conceptualized as an elongated, continuous and connected valley-shaped body. Our method captures the large-scale topographic features of fluvial incision into bedrock and the uncertainty in the positioning of the surface. Small-scale spatial variability is incorporated using Sequential Gaussian Simulation informed by geological analogs. Being stochastic, the methodology allows characterization of the uncertainty associated with positioning of the bedrock surface, by generating an ensemble of models via a Monte-Carlo analysis. This makes it possible to quantify the uncertainty associated with estimating the aquifer volume. We also discuss how this methodology may be used to better quantify the influence of uncertainty associated with defining the aquifer geometry on water resource assessment and management.

© 2013 Elsevier Ltd. All rights reserved.

## Software availability

Name of software: stochastic paleovalley interpolation V 1.0  
 Availability and cost: freeware downloadable from: <https://github.com/juancastilla/Paleovalley-Modelling.git> including documentation and demo datasets. The program is available as a set of Matlab functions and scripts. SGEMS

and mgstat are open-source software and can be downloaded at no cost from the developers' website.

Developers: Juan Carlos Castilla-Rho, Gregoire Mariethoz  
 Contact address: School of Civil and Environmental Engineering, University of New South Wales, Kensington Campus, Sydney, NSW 2052, Australia

Phone: +61 (0) 478074291

Email: [j.castilla@unsw.edu.au](mailto:j.castilla@unsw.edu.au)

Hardware required: 32- or 64-bit PC with Windows or Mac OS. We recommend a high-speed processor and at least 4 GB of RAM.

Software required: Matlab R2012b, mGstat geostatistical toolbox (<http://mgstat.sourceforge.net>), SGEMS geostatistical modelling software (<http://sgems.sourceforge.net>)

\* Corresponding author. School of Civil and Environmental Engineering, University of New South Wales, Kensington Campus, Sydney, NSW 2052, Australia. Tel.: +61 (0) 478074291.

E-mail addresses: [j.castilla@unsw.edu.au](mailto:j.castilla@unsw.edu.au) (J.C. Castilla-Rho), [gregoire.mariethoz@unsw.edu.au](mailto:gregoire.mariethoz@unsw.edu.au) (G. Mariethoz), [bryce.kelly@unsw.edu.au](mailto:bryce.kelly@unsw.edu.au) (B.F.J. Kelly), [m.andersen@unsw.edu.au](mailto:m.andersen@unsw.edu.au) (M.S. Andersen).

## 1. Introduction

The lack of spatial information is a prevalent issue for scientists and practitioners needing to assemble 3D models of geological regions. While carefully designed studies should rely on dense data collection campaigns, in practice economic and technical constraints often result in poor control of the quality and spatial arrangement of the data. Hydrogeology is particularly affected by this problem, as information mainly originates from localized data that sample a very small portion of the geological region of interest. In addition, subsurface morphology is usually heterogeneous, anisotropic and non-stationary. Furthermore, geoscientists can produce a range of interpretations from a single dataset, hence introducing knowledge bias and interpretational uncertainties (Bond et al., 2007). For all these reasons, geological uncertainty is often large, and significant research efforts are aimed at quantifying and capturing it for 3D structural, volumetric, facies and flow modeling applications.

Alluvial aquifers or basins are often modeled as a filling sequence overlying a bedrock surface (Hoyos et al., 2012; Jaireth et al., 2010; Whiteley, 2005). Their conceptualization is therefore controlled by the shape and geomorphology of the underlying structure, typically defined by a paleovalley bedrock surface. The aquifer then constitutes the permeable units of the unconsolidated sediments that overlie low permeability consolidated deposits or bedrock. However, the inherent limitations of geological datasets can make the task of characterizing bedrock surfaces challenging. This has significant implications for defining the transmissivity distribution in the aquifer or even for simpler characterization such as estimating the total volume of porous material in the reservoir.

Geostatistics is a widely used framework for making predictions at unmeasured locations from limited and sparsely arranged data. Geosciences and water resources rely heavily on geostatistics for spatial interpolation, with frequent use of kriging in its various forms (Li and Heap, 2011). A limitation of kriging is that it relies on assumptions of stationarity and smoothness, and limited representation of anisotropy (such as zonal anisotropy). Although traditional geostatistical methods can include data sources such as digital elevation models (DEMs), wells and geophysics, it is often found that representing complex geometries of geological systems is difficult (Neuweiler and Vogel, 2007; Zinn and Harvey, 2003). These issues are general and arise when working on structures having characteristics of non-stationary and meandering geometries, such as 3D groundwater models demanding realistic bedrock surfaces. Some of the approaches that have been proposed to model geological complexity include multiple-point statistics (Guardiano and Srivastava, 1993; Hu and Chugunova, 2008; Mariethoz and Kelly, 2011), object-based methods (Haldorsen and Chang, 1986) or complex forms of indicator simulation such as the pluriGaussian method (Le Loc'h et al., 1994; Mariethoz et al., 2008). Although these methods are appropriate for 3D gridded facies models, they are not always applicable to modeling geological surfaces, which are continuous and strongly non-stationary.

The literature on spatial interpolation of topographic datasets in meandering, non-stationary valley-shaped landscapes presents a series of solutions and customizations to improve the performance of simple interpolators when applied to such data (Nordfjord et al., 2005). One successful approach has been to transform the datasets to a channel-oriented coordinate system prior to interpolation (Legleiter and Kyriakidis, 2008; Merwade, 2009; Merwade et al., 2006, 2005). This coordinate conversion, however, is more appropriate for dense datasets and requires accurate definition of the channel centerline, often a time-intensive task (Goff and Nordfjord,

2004). Unfortunately, in hydrogeology the data is frequently too sparse for this method to be successful. Another general principle often used to improve topographic reconstructions is the concept of separating trend from the data using empirical functions. This idea has been the focus of recent studies related to river bathymetry modeling (Legleiter and Kyriakidis, 2008; Merwade, 2009), allowing subsequent application of isotropic interpolation. These methods still present challenges, particularly in addressing non-stationarity (Merwade, 2009) and their suitability to site-specific data. Even though some studies derive generic trend functions using modern analogs (Allan James, 1996), their applicability to different settings should be dealt with caution. For instance, the morphological differences between fluvial and glacial environments may invalidate the applicability of a method derived for a specific environment (Anderson et al., 2006; Graf, 1970; Li et al., 2001). Therefore, a general methodology is needed to fully extract trends from available data, avoiding loss of information typically occurring during curve-fitting procedures. Also relevant to this work, is the use of random fields through Sequential Gaussian Simulation (SGS). Gringarten et al. (2005) use this approach to simultaneously confer realistic geological features to topographic models, while conditioning to well-log data. As a by-product of this workflow, several possible realizations are obtained which can be used to convey quantitative measures of uncertainty.

In recent years, many authors have demonstrated that aquifer conceptualization is responsible for a significant proportion of the uncertainty in groundwater model predictions (Bond et al., 2007; Bredehoeft, 2005; Neuman, 2004; Poeter, 2007; Rojas et al., 2010; Zeng et al., 2013). To date however, the specific problem of generating 3D reconstructions of paleovalley geomorphology with sparse data has received little attention. The goal of this paper is to model uncertainty related to the alluvium/bedrock interface caused by limited subsurface information, which is often an important source of predictive uncertainty (Poeter, 2007; Refsgaard et al., 2012). In this regard, multi-realization methodologies have a proven track-record in the quantification of uncertainty due to data limitation and other factors (Refsgaard et al., 2012; Trolldborg et al., 2007). This last point highlights the need for specialized geostatistical algorithms capable of generating multiple realizations of alluvium–bedrock interfaces.

In this paper, we address the challenge of integrating, in an automated workflow, the various pieces of information available for the characterization of alluvial-aquifer bedrock surfaces using a stochastic multi-realization approach. We adopt a hybrid modeling framework (Bertoncello et al., 2013; Dubrule, 1993; Michael et al., 2010), which combines different approaches and data types to tailor the modeling workflow to a specific geologic environment. Fig. 1 illustrates the general problem of a bedrock surface overlain by valley-filling unconsolidated sediments, along with the different types of data typically available for a geological modeling. The data sources considered here are:

1. Lithological data from boreholes that intersect the bedrock, as well as those that do not intersect it but provide an estimate of the upper bound of the alluvium–bedrock interface,
2. Geophysical surveys providing cross-sections of the bedrock surface,
3. Digital elevation models (DEMs), and
4. Conceptualization of bedrock geometry as elongated, continuous and V-shaped, typical of fluvial valleys.

Each data source brings information of a different nature. Lithological well-logs inform the depth to bedrock quite accurately; however they are typically not numerous enough to

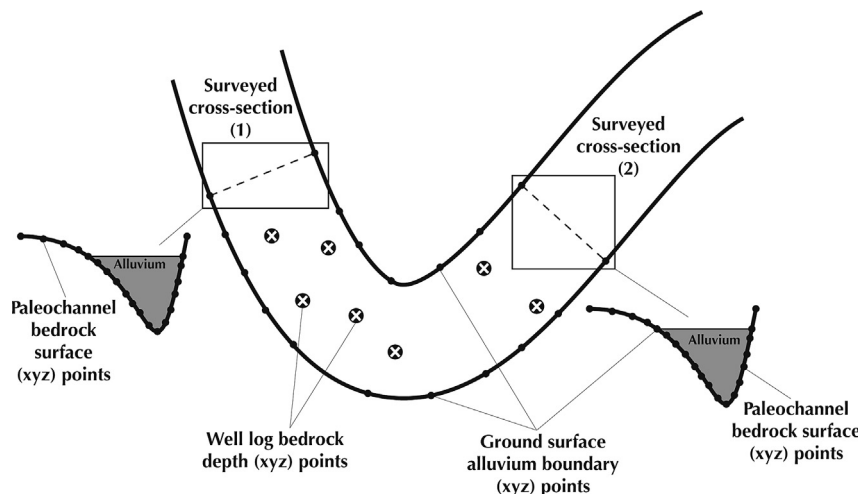


**Fig. 1.** Illustration of different types of input data typically needed for mapping buried bedrock surfaces.

reliably infer the spatial variability and non-stationarity (or to determine horizontal variograms). Geophysical surveys, such as electrical resistivity or gravimetric profiles, are a useful source of information since they delineate the bedrock depth and non-stationarity along certain cross-sections. Surface geophysics however suffers non-uniqueness and is prone to interpretational errors, which may be an important source of uncertainty (Kirsch, 2008). Furthermore, these cross-sections may be relatively far apart and often do not cover the entire domain. This is where assumptions have to be made about the continuity of the morphological features between observed profiles. Such assumptions need to be guided by established geomorphological concepts about the structure of paleovalleys to realistically combine well and geophysical data.

Most of these morphological concepts can be represented by geological analogs obtained from bedrock outcrops, experimental simulations, or observations from the present landscape. Geological analogs have been widely used in geological modeling (Alexander, 1993; Caers and Zhang, 2004; Enge et al., 2007; Friedmann et al., 2003; Grammer et al., 2004; Jones et al., 2008; Liu et al., 2004; Pringle et al., 2006; Tye, 2004), although they have not been applied to the specific problem of reconstructing paleovalley surfaces. Our method extends the use of the analog approach for this purpose, including typical characteristics of fluvial incision into bedrock such as profile convexities, knickpoints and irregular scour patterns (Gardner, 1983; Phillips and Lutz, 2008; Seidl and Dietrich, 1993; Shepherd and Schumm, 1974; Stock and Montgomery, 1999; Whittaker et al., 2007).

This study develops a methodology that is demonstrated on incised fluvial valleys, but with minor modifications the method is generally applicable for generating surfaces of glacial valleys through to ocean trenches. The paper outlines the overall workflow of our paleovalley bedrock interpolation technique, investigating how it addresses the challenge of integrating data of different nature, scale and resolution. Two examples are presented. The first is a synthetic meandering channel generated using a generic sine wave. In this example, the methodology is validated through an uncertainty characterization exercise, where we assess the potential to capture large-scale morphological variability. The second example uses lithological well-logs and gravity survey data from the Azapa valley aquifer in Northern Chile, representing a typical case of limited field data. This second application also demonstrates the incorporation of small-scale spatial variability using geological analogs.

Our methodology is intended to complement available methods and improve uncertainty characterization in groundwater modeling. The methodology may be used to better evaluate the effects of uncertainty and data limitation on water resource assessments, because it addresses an important and often overlooked component of a hydrogeological conceptual model: the bedrock–alluvium interface. This method is sufficiently simple and economic to be applied in resource-limited projects.

## 2. Methodology

The core of our approach is to pair each point of the unknown bedrock surface to locations on geophysical cross-sections located on either side of it. The pairing is chosen such that a simple interpolation method enables smooth propagation of the geophysical profiles, while ensuring continuity of the overall paleovalley shape. Pairing is accomplished by first determining the channel axis, or centerline, and then propagating locally observed features along the channel axis.

The approach is subdivided into three main steps:

1. Construct one or more trend surfaces consistent with known bedrock data. These trend models aim to capture the large-scale (first-order) topographic uncertainty of the paleovalley;
2. Generate a series of stochastic, equally likely error surfaces corresponding to departures from the trend surface. The stochastic component is based on geological analogs, and is used to impair natural variability to the bedrock surface. The error surface also confers geological realism and local conditioning to known bedrock elevations (typically well-log data). Its aim is to capture the small-scale (second-order) morphological uncertainty; and
3. Combine the trend surfaces and stochastic models to create a final ensemble of conditional model realizations.

These steps are developed in the following sections.

### 2.1. Trend surfaces

#### 2.1.1. Input data

Input data consists of geological information stored in a Cartesian coordinate system. Firstly, we focus on the aquifer boundary ( $x,y,z$ ) data, depicting the limit between the alluvial aquifer and outcropping bedrock. These data can be obtained from several sources such as aerial photographs, digital elevation models (DEMs), geological maps or existing GIS databases. Secondly, our methodology takes into consideration cross-sections, which delineate 2D slices of the bedrock at each geophysical transect. The latter are also incorporated as ( $x,y,z$ ) points and can be inferred from either gravimetric, seismic, electromagnetic and resistivity surveys, or a combination of them. Fig. 1 summarizes the typical forms of input data. We assume, as is often the case, that considerable spacing exists between transects. It is these sparser data arrangements that are challenging for conventional interpolation.

#### 2.1.2. Finding the channel centerline

In hydrological studies such as modeling of river bathymetry, where the topography is accessible and data density is often large, it is generally possible to determine the thalweg and use it as a centerline (see Merwade et al., 2006).

However, in the case of subsurface topography the location of the minimum elevation line (analogous to the thalweg in hydrology) is unknown. To address this problem, we trace the channel centerline along the length of the aquifer by employing the skeletonization algorithm used in mathematical morphology (Gold and Snoeyink, 2001; Gonzalez et al., 2009; Haunert and Sester, 2007; Niblack et al., 1992; Serra and Soille, 1994). A similar approach has been used in the context of river modeling (Bangmei et al., 2010).

The skeletonization method obtains the medial axis of a convex region by sequential thinning of a geometrical shape until the resulting figure is one pixel thick, while preserving the connectivity properties of the original shape, as shown in Fig. 2a–c. This algorithm often produces unwanted features protruding from the extracted centerline, known as spurs or parasitic components (Bangmei et al., 2010; Gonzalez et al., 2009), which are easily removed during a post-processing step. Since the skeletonization and spur removal sequence produce a unique result, the channel centerline can be obtained automatically and unambiguously (Fig. 2d). Defining the paleochannel centerline in this manner is a key component in the proposed method, because it allows generating a customized interpolation grid that follows the sinuosity and meandering nature of the fluvial depositional system.

The skeletonization algorithm is capable of producing a centerline from any type of irregular shape depicting the general outline of the region of interest. In its simplest form, this outline would correspond to outcropping bedrock at the outer edges of the paleovalley. Alternatively, in the absence of outcrops, a suitable outline may be obtained from the interpretation of geophysical surveys, geological maps or aerial photographs.

#### 2.1.3. Uniform grid space discretization

To implement customized grids within our interpolation workflow, we combine the centerline extraction routine with the concept of interim cross-sections (Goff and Nordfjord, 2004; Merwade et al., 2008). This facilitates the automatic definition of a uniform grid conforming to the specific paleochannel geometry being studied. Interim cross-sections are created between surveyed transects, that are equally spaced and orthogonally oriented with respect to the centerline (Fig. 3a,b). The number of interim sections to be created depends on several factors including paleochannel sinuosity, distance between surveyed cross-sections, desired along-channel resolution and shape of the aquifer boundary. In the context of river bathymetry, Merwade et al. (2008) comment on the maximum number of interim cross-sections that can be created in this manner, to avoid two adjacent cross-sections intersecting.

At this point, all interim cross-sections are discretized in a fixed number of interpolation nodes (Fig. 3a,b). This number, representing the level of discretization, depends on the desired across-channel model resolution. The lateral resolution should be at least equivalent to that of the surveyed cross section data. However, a larger number of nodes are recommended, as it does not dramatically increase computation times due to the simplicity of the final interpolation step described below. Given that the channel width can vary along its profile and that the number of nodes is fixed, the spacing between two neighboring nodes within interim sections may vary along the channel. The (x,y) location of each of these nodes is stored in two separate  $M$  by  $N$  rectangular matrices, where  $M$  defines the number of interpolation nodes and  $N$  is the number of interim cross-sections, respectively (Fig. 3b). A matrix of the same dimensions ( $Z$ ) is used to separately store the elevation data.

#### 2.1.4. Locating the trajectory of channel minimum elevation

Once the uniform interpolation grid has been defined, we consider the problem of maintaining coherent paleovalley morphology within the model. This can be

understood as conserving the typical elongated U or V shape of the bedrock while allowing for non-stationarity (i.e. a general longitudinal trend in the slope of the valley bottom elevation and the meandering nature of the valley). For this purpose, we identify a valley minimum elevation on the known cross-sections and propagate it through the matrix representation of the bedrock surface  $Z$  (see Fig. 3c,d).

If the discretization of the interpolation grid  $Z$  is different from the resolution of the transect data, the data are interpolated using cubic splines or linear interpolation. This information is stored in the first and last columns of  $Z$  (columns 0 and  $N$ ). The row positions of the  $z$  values corresponding to the minimum channel elevation are identified on these first and last columns. Then, a linear interpolation of these indexes is performed, generating a vector of row index locations for each interim cross-section. The resulting vector corresponds to the expected location of the valley bottom along the model space. A graphical representation of this procedure is presented in Fig. 3d.

#### 2.1.5. Non-uniform grid adaptation for pairing of cross-section data points

After completing the task of estimating the paleovalley minimum elevation axis, the model space is discretized into a non-uniform grid in preparation for interpolating the remaining bedrock surface. Previous steps have located the nodal position of the valley minimum for each interim cross-section, but often the number of nodes on each side of the minimum will not be equal (see Fig. 3c,d) due to the generally asymmetrical shape of paleovalleys. In the previous step, the uniform grid was established exclusively to locate the points defining the valley minimum. Now, the total number of interpolation nodes on any interim cross-section is halved and placed on each side of the valley minimum (Fig. 3f). This new non-uniform interpolation grid maintains the number and location of interim cross-sections defined earlier, but the number and location of nodal points is redefined. The above grid adaptation is performed automatically, and illustrated in Fig. 3c,d (before rediscretization) and Fig. 3e,f (after rediscretization).

Maintaining equal number of paired interim cross-section nodes across the model is a key feature in the algorithm for several reasons. First, this allows pairing each node with others located either upstream or downstream. The concept of having a paired non-uniform interpolation grid is analogous to a fictitious longitudinal cross-section that travels from one (known) surveyed transect, which then morphs downstream and finally matches a downstream surveyed transect. This corresponds to an explicit assumption of valley continuity as an elongated U or V shape guided by geophysical cross-section data. Second, pairing allows significant reduction in computational resources, as simple linear interpolation procedures become sufficient once the non-uniform grid is created. Third, a paired grid space allows storing and manipulating the data in rectangular matrices (Fig. 3f), without the channel-oriented coordinate transformation proposed by several authors (Goff and Nordfjord, 2004; Legleiter and Kyriakidis, 2008; Merwade, 2009).

#### 2.1.6. Simple spatial interpolation using channel distance

As a result of discretizing the model grid in a paired manner, spatial interpolation of bedrock elevation proceeds by propagating surveyed data along this grid in the upstream and downstream directions. By propagating morphological data along the channel direction, we are able to enforce our main morphological assumptions, such as connectivity of the deepest portions of the bedrock surface for a fluvial valley, the general elongation of the system and a V-shape or U-shape cross-section (depending on the measured cross-sections).

Meandering geometries such as paleochannels often have non-convexity: a line connecting two points in the paleovalley may lie outside the paleovalley boundaries. Therefore, Euclidean distance is not an appropriate distance metric for interpolation. To solve this problem, we incorporate the concept of water distance as defined in

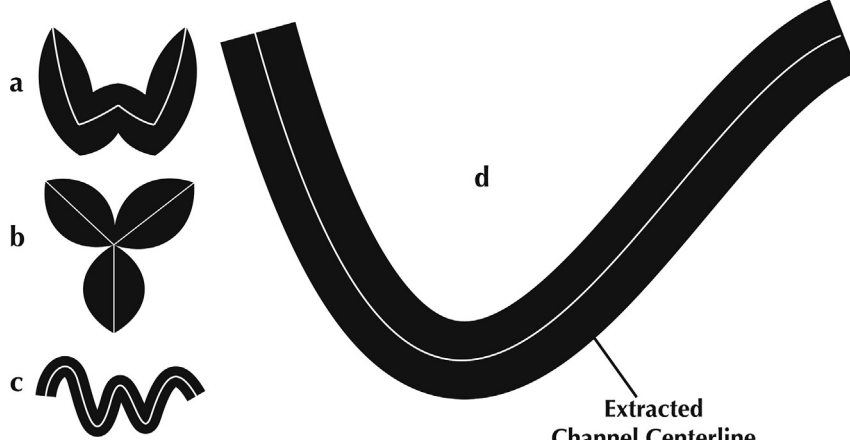


**Fig. 2.** Examples of the use of the skeletonization method from mathematical morphology. (a)–(c) Schematic representation of skeleton extraction from binary images; (d) application on a meandering channel for centerline delineation.

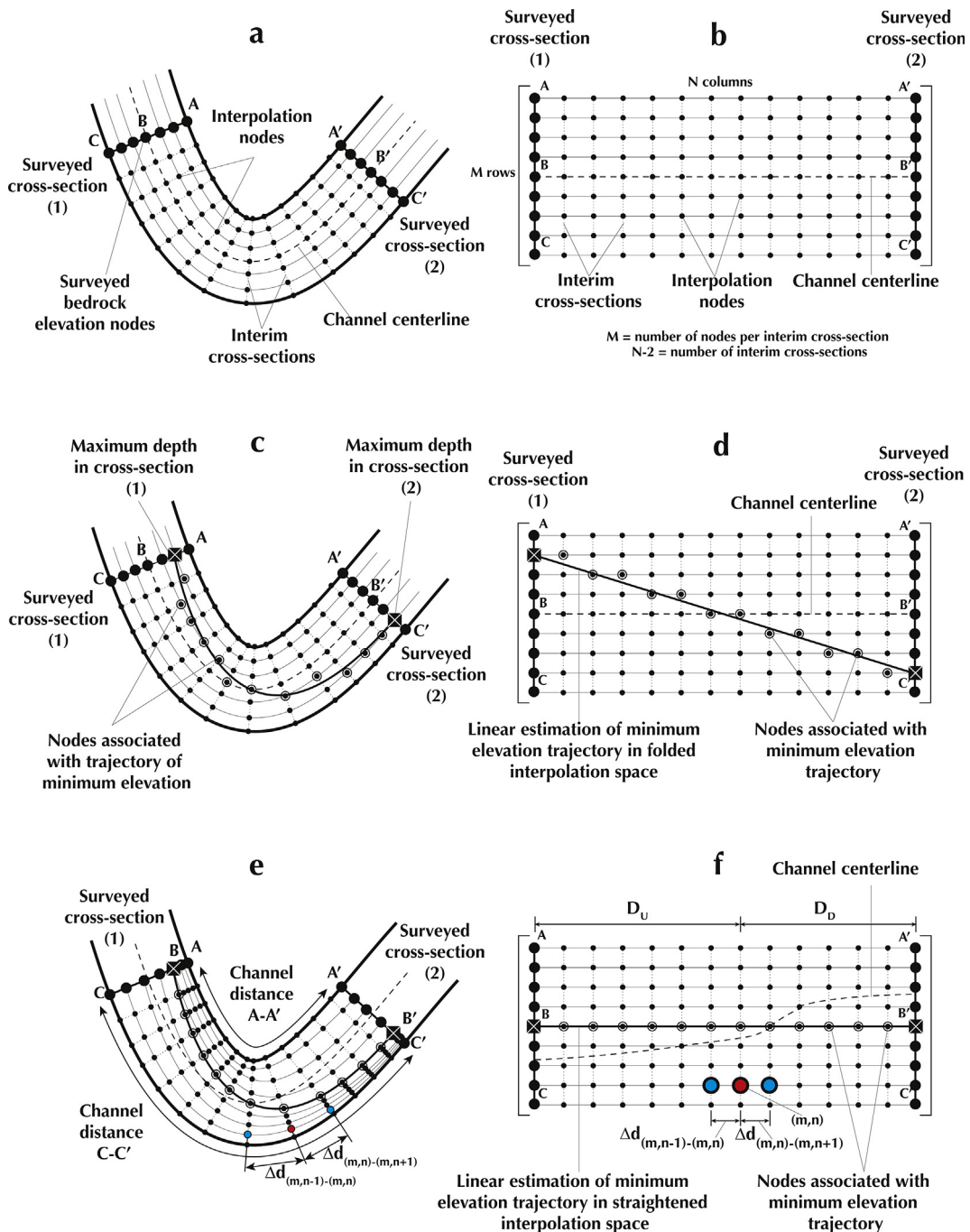


**Fig. 3.** Illustration of the algorithm. (a), (b) Uniform discretization based on the extracted centre line, location of survey data, interim cross-sections and its matrix representation; (c), (d) locating the line of steepest descent within the uniform grid; (e), (f) grid adaptation by pairing nodes between interim cross-sections and notation used to calculate channel distances.

(Rathbun, 1998), but apply it in a slightly different manner. We define the notion of channel distance as the length of the path connecting two cross sections, which has the following characteristics: (1) is fully contained within the alluvial-aquifer boundaries, and (2) follows the natural sinuosity of the paleovalley.

Incorporating the concept of channel distance is simplified by using the matrix formulation presented in Fig. 3. Fig. 3e shows a synthetic channel segment with a series of interim cross-sections, surveyed transects and interpolation nodes. For a meandering system, the channel distance between two paired nodes depends on the relative location within the cross-section. For instance, channel distance A–A' (inside of bend) is much shorter than distances B–B' (channel centerline) and C–C' (outside of bend). These distances are estimated by summing all individual linear segments located between two paired nodes, as shown in Fig. 3e,f. Channel distances  $D_U$  (distance to upstream surveyed transect) and  $D_D$  (distance to downstream surveyed transect) are then given by:

$$D_{U(m,n)} = \sum_{k=2}^n \Delta d_{(m,k-1)-(m,k)} \quad (1)$$

$$D_{D(m,n)} = \sum_{k=n}^{N-1} \Delta d_{(m,k)-(m,k+1)} \quad (2)$$

where  $m$  is the node index,  $n$  is the cross-section index and  $N$  is the total number of cross-sections (including the two surveyed transects). The final spatial interpolation is obtained by creating matrices containing  $D_{U(m,n)}$  and  $D_{D(m,n)}$  values for each node. The elevation at an interim node is computed as a weighted average of the corresponding (paired) upstream and downstream survey nodes, using channel distances  $D_U$  and  $D_D$ .

$$z_{(m,n)} = \frac{z_{(m,1)}D_{U(m,n)} + z_{(m,N)}D_{D(m,n)}}{D_{U(m,n)} + D_{D(m,n)}} \quad (3)$$

where  $z(m,n)$  is the topographical elevation at any given node. Outside surface nodes for each interim cross-section (i.e. next to the land surface channel boundary) adopt the known elevation of the bedrock–alluvium boundary. Treating surface boundary nodes in this manner offers a simple way of integrating the paleovalley bedrock model with contiguous DEM topographic data. Ultimately, a matrix of interpolated  $z$  values is obtained which defines the shape of the paleovalley bedrock surface.

One common problem related to the acquisition of geophysical datasets is the occurrence of natural or anthropogenic obstacles that prevent the ideal location of sampling points. As a consequence, geophysical transects are rarely orientated perpendicular to the valley axis. In these circumstances, interim cross sections are extended past the surveyed transects, elevations are interpolated using Eq. (3), and finally the nodes outside the region of interest are clipped from the model.

## 2.2. Bedrock stochastic deviations

We use stochastic topographic simulations superimposed on the bedrock trend surfaces, in order to reproduce the small-scale variability of subsurface topography and to characterize the related (second-order) geological uncertainty. These stochastic realizations have a zero mean, and add autocorrelated noise on top of the trend without changing its overall shape. Multiple plausible representations of the bedrock shape are calculated to quantify this second-order source of uncertainty. In this study we use Sequential Gaussian Simulation as a perturbation method, although any continuous geostatistical simulation method would be suitable. SGS uses a parametric model (the variogram) that describes the small-scale variability of the bedrock topography. Our implementation employs SGEMS (Remy et al., 2009) with the mGSTAT interface (Hansen, 2004) to generate multiple realizations of conditional topographic variability for the paleovalley surface. In the particular case of SGS, small-scale topographic variability (i.e. the error surface) is assumed to have a Gaussian distribution with parameters obtained from the kriging mean and variance. In our method, variograms are the chosen tool used to transfer the analog information into the bedrock surface predictions. They allow us to confer a realistic variability valley profile, resembling the typical characteristics of river incision into bedrock, such as a longitudinal profile presenting irregularly-spaced scour highs and lows (Shepherd and Schumm, 1974). SGS however requires valid assumptions about the variogram model to be employed, which ultimately depends on site-specific geological features. One option is to utilize the topographic variations observed in local bedrock outcrops. This strategy, along with alternative approaches, is discussed later in this paper, when applying the methodology to the reconstruction of a real paleovalley bedrock surface in Chile.

Since SGS is a conditional method, it is used to impose further constraints on the generated bedrock surface, such as elevations at points where the bedrock location is known from lithological well-logs and known elevations along the ground-surface/paleovalley boundary (e.g. local outcropping). SGS-simulated deviations from the trend are conditioned to the difference between a known bedrock elevation and the elevation of the trend surface at the surveyed location, resulting in modeled bedrock elevations corresponding to the measured values. Since the interpolated trend is already conditional to intersections of the bedrock with the surface topography, the boundaries of the domain are conditioned to a value of zero.

In addition to conditioning using lithological well-logs, in certain cases it may be desirable to introduce conditioning to the paleovalley minimum elevation of the 2D trend surface. For example, the modeler can impose different types of erosion patterns along the longitudinal profile of the valley, corresponding to distinct assumptions about the incision process. These assumptions may be related to different conceptualizations about the sediment and rock strength controls or climate regimes during the development of the valley; for examples see Finnegan et al. (2005), Gardner (1983), Shepherd and Schumm (1974), Sklar (2007). By using this approach many of the features found in modern and experimental analogs of bedrock incision may be incorporated into the models. Most importantly, the approach offers a means of exploring the smaller scale morphological uncertainties in the estimation of the paleovalley shape.

Although in this study we focus on alluvium-filled incised bedrock valleys, simple customizations of this step allow for application to other types of paleochannels, such as glaciated valleys. Glacial valleys, in contrast to fluvial V-shaped valleys, are characterized by U-shaped troughs and a smoother longitudinal profile with a larger-scale erosional footprint (Anderson et al., 2006; MacGregor et al., 2000). Therefore, for other morphologies the modeler may choose variograms with a higher range and smaller variability to impair general smoothness of the glacial incision signature along the valley (Anderson et al., 2006).

The final step is to superimpose the trend and stochastic components of the model; SGS realizations are combined with one or many trend surfaces, producing multiple equally likely realizations of the bedrock surface. Fig. 4 presents a complete flowchart of our algorithm, describing the sequence of steps leading to a set of stochastic realizations of the paleovalley topography.

## 3. A synthetic example

### 3.1. Input datasets

For the synthetic example, we consider a simple sine wave channel and four synthetic generic surveyed cross-sections (Fig. 5a,b). Cross-section six (CS6) is included in the analysis to show the effect of a stronger variation in channel depth.

### 3.2. Trend surfaces

The sequence of steps leading to a trend model is summarized in Fig. 5c–l, starting from extraction of channel centerline through skeletonization and spur removal (Fig. 5c–e); creation of interim cross-sections with subsequent location of bedrock minimum elevation (Fig. 5f) and final interpolation (Fig. 5g) to obtain a trend surface.

A visual comparison of 2D trend surfaces for different pairs of surveyed cross-sections (Fig. 5g–l) demonstrates that the method is capable of producing non-stationary trend models of the paleovalley. The trend model varies depending on which cross-sections are considered. The lateral position of the deepest point of the bedrock surface is different for each case, because it changes position between surveyed transects. Overall, the reconstructed channel corresponds to our earlier definition of channel continuity: consistent, elongated bodies maintaining longitudinal coherence of the channel morphology.

A trend surface with stronger elevation gradient is presented in Fig. 5h, showing the ability to reproduce both linear (bed slope) and non-linear (cross-section shape) trends. The resolution of the trend model can be customized according to specific modeling needs, as both the number of interim cross-sections and transverse interpolation nodes are parameters defined by the user. From our tests, interpolations considering higher model resolution only generate marginal increases in computation time. Finally, we present the modularity of this approach when three trend models are stitched together producing consistent fits (Fig. 5k–l). This demonstrates how trend surfaces can be constantly updated as new field data is collected, and easily incorporated into existing models. In addition, comparison of Fig. 5g and l illustrates how the final trend surface improves as more survey cross-sections are considered and combined through the stitching process.

The need to define the trajectory of the channel minimum is presented in Fig. 6a, which shows a surface that has not been constrained to have the deepest values connected along a line of steepest descent. Here, the trend surface is a smooth transition between the two survey profiles, with a flat section in the middle. In contrast, Fig. 6b shows that the inclusion of the minimum valley trajectory by the process of grid adaptation and node pairing ensures that the model conforms to the general morphological understanding of the system. This demonstrates the importance of incorporating the geomorphological knowledge of the overall shape associated with a buried paleovalley system. Moreover, it is possible to consider alternative interpretations of the geophysical data to obtain alternative trend models, for example using a Bayesian approach. Combinations of different paleovalley axis trajectories with several geophysical interpretations will produce an even larger ensemble of trend models, with greater variability.

### 3.3. Adding the stochastic component

Generating the stochastic component of the valley can be approached in several ways, depending on how the variability surfaces are conditioned to hard data. Before generating stochastic data, DEM elevation data needs to be imposed to the surface

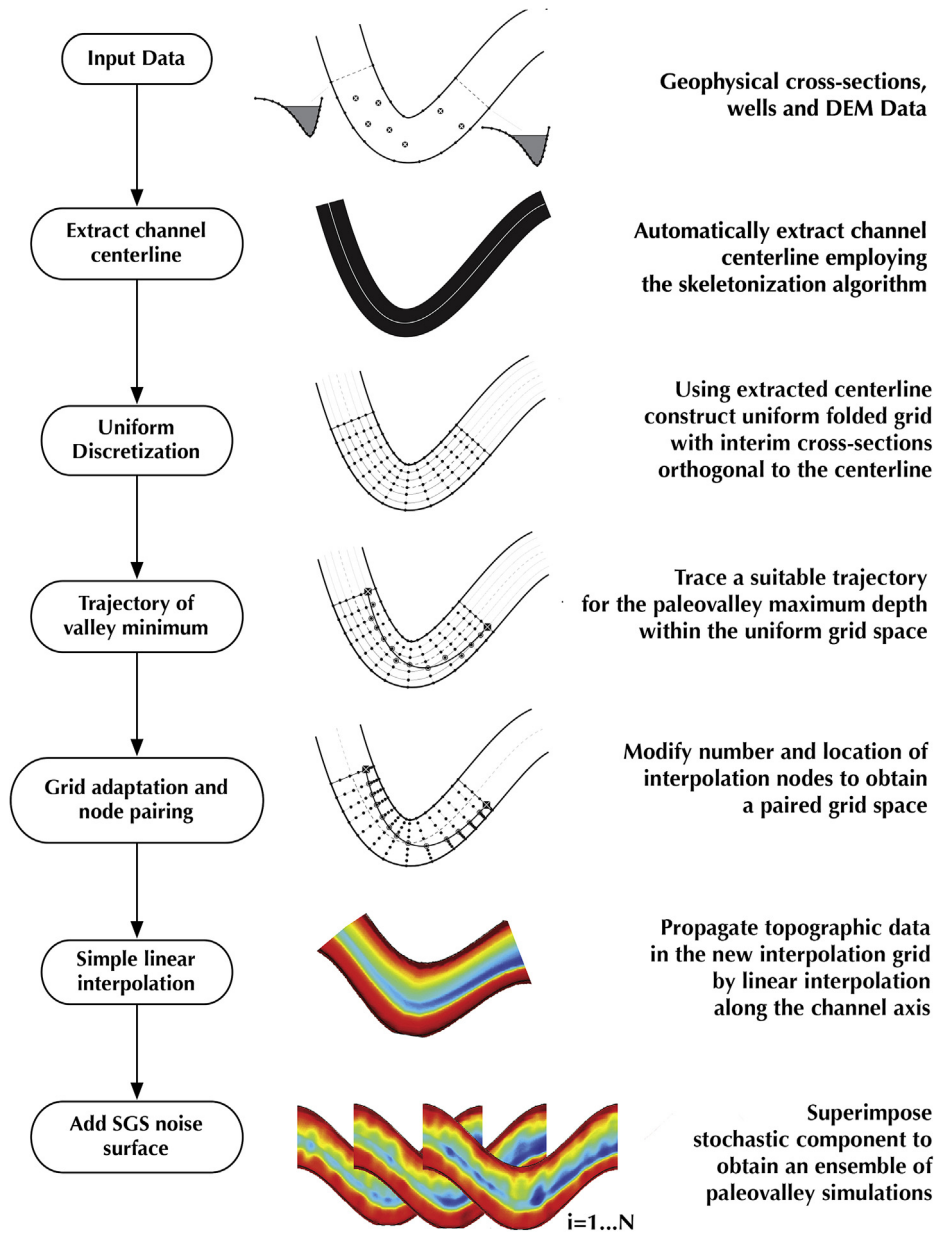


**Fig. 4.** Flowchart representation of the algorithm developed for the stochastic construction of paleovalley bedrock surfaces from DEMs, geophysics and well-log data.

expression of the aquifer boundaries as conditioning data, which for most locations can be obtained from raster satellite imagery. Fig. 5m shows the result of combining the trend surface of Fig. 5h with a SGS model of small-scale variability, and the characteristic fluvial incision signature consisting of scour lows that is impaired (Shepherd and Schumm, 1974). Here, it is important to note that although the SGS surface is stationary, along the longitudinal axis of the valley the resulting scour highs and lows are irregularly-spaced. Alternatively, the SGS realizations can be locally conditioned to depict different types of incision processes. Fig. 5n shows one realization with a smoother incision footprint (compared to Fig. 5m) along its longitudinal profile, obtained by constraining the SGS surface along the paleovalley bottom axis.

Fig. 5m,n shows only one of the many possible stochastic realizations that can be obtained. For the models presented in Fig. 5m,n, an arbitrary set of Gaussian model parameters were used, however in a real study the variogram parameters can be inferred from the topographic variability of outcropping bedrock or

any other type of geological analog (more details and discussion in Section 4.3). Finally, the SGS noise surface can be conditioned to bedrock depth data from wells, as presented in Section 4, where the methodology is applied to the reconstruction of a real paleovalley in Chile.

### 3.4. Characterization of large-scale uncertainties

Although SGS allows impairing small-scale (second-order) variability, it does not account for large uncertainties (first-order) in the trend itself. An uncertainty analysis was done based on multiple synthetic paleovalley realizations to assess large-scale topographic uncertainties for varying sampling densities. This analysis can also provide some insights on how to select future sampling locations.

To compare the uncertainty results with a reference we constructed a synthetic paleochannel reproducing some essential characteristics of fluvial bedrock incisions such as: (1) knickpoints;

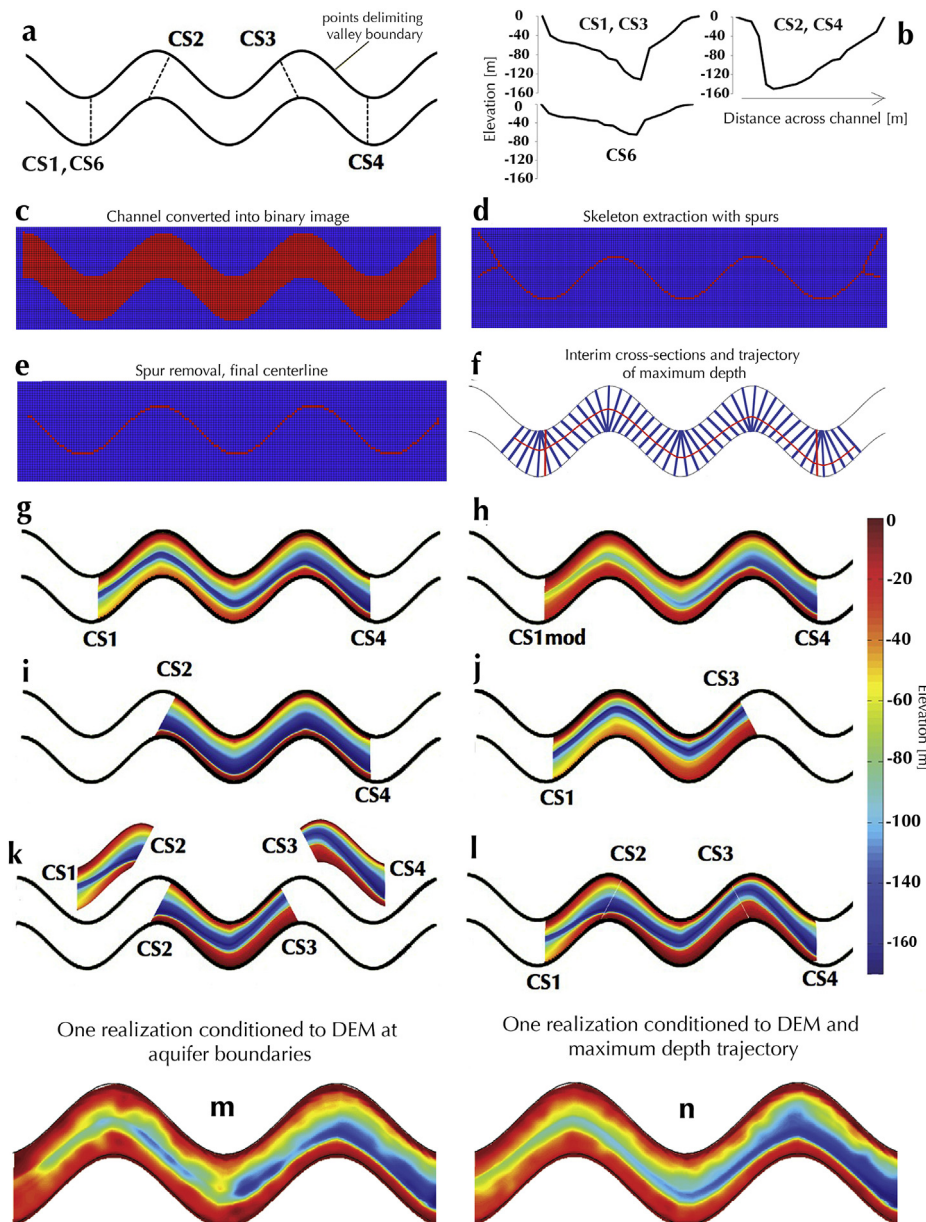


**Fig. 5.** Stepwise reconstruction of a synthetic paleovalley. (a), (b) Synthetic cross-sections; (c) paleochannel converted into binary image; (d) centerline extracted by skeletonization, with spurs; (e) centerline after spur removal; (f) interim cross-sections and linear approximation of maximum depth of the paleovalley; (g)–(l) trend surfaces for different combinations of synthetic cross-sections; (m) final reconstruction after addition of SGS noise to the trend surface, conditioned only to DEM elevations at the aquifer boundary; (n) final reconstruction after addition of SGS noise to the trend surface, conditioned to DEM elevations at the aquifer boundary and maximum depth of paleovalley from the trend surface. Note in (m) the characteristic signature of bedrock incision, comprised of scour highs and lows. (h) is the trend surface for plots (m) and (n).

(2) irregularly-spaced bedrock scour highs and lows; (3) longitudinal profile convexities; and (4) non-stationary longitudinal and transverse incision, as shown in Fig. 7 (Gardner, 1983; Phillips and Lutz, 2008; Seidl and Dietrich, 1993; Shepherd and Schumm, 1974; Stock and Montgomery, 1999; Whittaker et al., 2007). Although this is a specific test example, it represents a typical and challenging geological scenario that is likely to be encountered in the field.

The uncertainty in capturing the longitudinal profile and incision morphology of the paleovalley was assessed, as illustrated in Fig. 8. These plots show the rapid convergence of the methodology, and its capacity to capture the large-scale topographic uncertainty with relatively few surveys ( $s > 4$ ). Fig. 8 also shows that an accurate estimation of the aquifer volume does not necessarily correspond to an accurate prediction of the longitudinal profile.

Using the fully known reference bedrock surface described above, we evaluated the effect of sparser survey datasets on the topographic uncertainty. Fifty random realizations were generated for a relatively dense sampling strategy, and an equal number of random realizations for progressively thinned versions of this dataset, with the final case consisting of a single cross-section. Each of the fifty realizations within a specific sampling density represents a random spatial arrangement of a fixed number  $s$  of survey locations. Fig. 9 presents three of those realizations, obtained for a sparse ( $s = 1$ ), two intermediate ( $s = 4$  and  $s = 10$ ) and one dense ( $s = 25$ ) sampling strategy. By analyzing the ensemble of realizations, it was possible to characterize the uncertainties associated with cross-section density and cross-section spatial configuration.

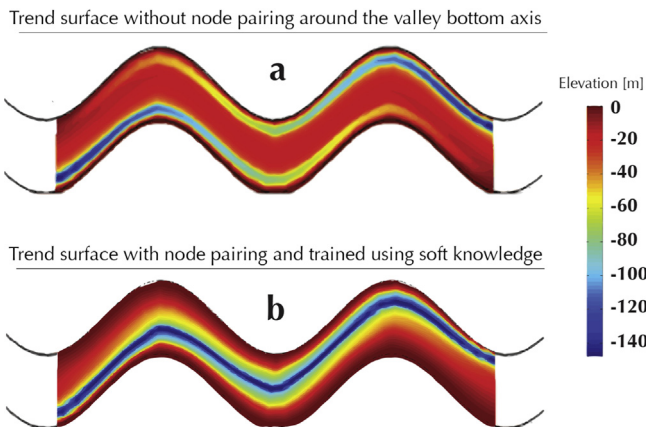


**Fig. 6.** Visual comparison of employing an adaptive grid with paired nodes. (a) No pairing; (b) paired nodes around the line of steepest descent. Note how this achieves and elongated, V-shape valley and enforces continuity.

The top part of Fig. 9 shows a selection of three random realizations for each sampling density. Although for a single survey ( $s = 1$ ) the realizations are highly variable, a slight increase in sampling locations ( $s = 4$ ) manages to capture the main features of the real topography, particularly the location of the knickpoint. For  $s = 10$  the knickpoint is fully constrained by the realizations, and for  $s = 25$  the variability between realizations is marginal and localized. A closer inspection of Fig. 8 reveals that the most accurate realizations within each ensemble (#50 in Fig. 8) have one common feature: they sample the main non-stationarities of the paleovalley, the knickpoint's lip and foot. In this regard, selecting sampling locations using prior geological knowledge depicting the possible location of knickpoints along the profile, has the potential to reduce field costs.

The bottom part of Fig. 9 shows the spatial patterns of topographic uncertainty for each sampling ensemble, visualized by the ensemble mean and standard deviation summary statistics. On one hand, the ensemble means reinforce that this method constrains the realizations to the reference topography after a relatively small number of surveys ( $s = 4$ ). The ensemble standard deviations provide insights about the spatial structure of uncertainty. These plots show that for a sparse data arrangement, the uncertainty is largest in the central part of the model and around the deepest portion of the paleovalley. It is interesting to note that for  $s = 1$ , the area of largest variability extends beyond the location of the knickpoint. In fact, for  $s = 1$  the largest uncertainty is not the knickpoint foot, but the bottom of the valley at the central meander (location A, Fig. 9). This is simply because a single survey cannot reproduce the knickpoint feature using our methodology. Increasing the sampling to  $s = 4$  clearly reveals three distinct sources of uncertainty: the knickpoint (location B, Fig. 9); the incision scour signature along the longitudinal profile (location C, Fig. 9); and portions of the valley with sharp transverse topography (location D, Fig. 9). Further increasing the number of surveys shows that the topographic variability due to the knickpoint (B) is reduced by  $s = 10$  and eliminated by  $s = 25$ , however the remaining uncertainties (C and D) remain almost unchanged. Overall, this shows that by increasing the number of surveys it is possible to capture the large-scale topographic trend, but not the small-scale morphological uncertainties. Uncertainties (E) and (D) in Fig. 9 are due to the discretization of the model and the quality of the geophysical prospecting method, respectively. While (E) can be targeted by increasing the number of interpolation cross-sections, (D) will require higher transverse survey resolutions. Finally, the small-scale topographic uncertainties such as (C) are the target of the SGS step of our methodology, which is developed in Section 4.

An important and often highly uncertain parameter in groundwater resource estimates is the total aquifer volume. Non-

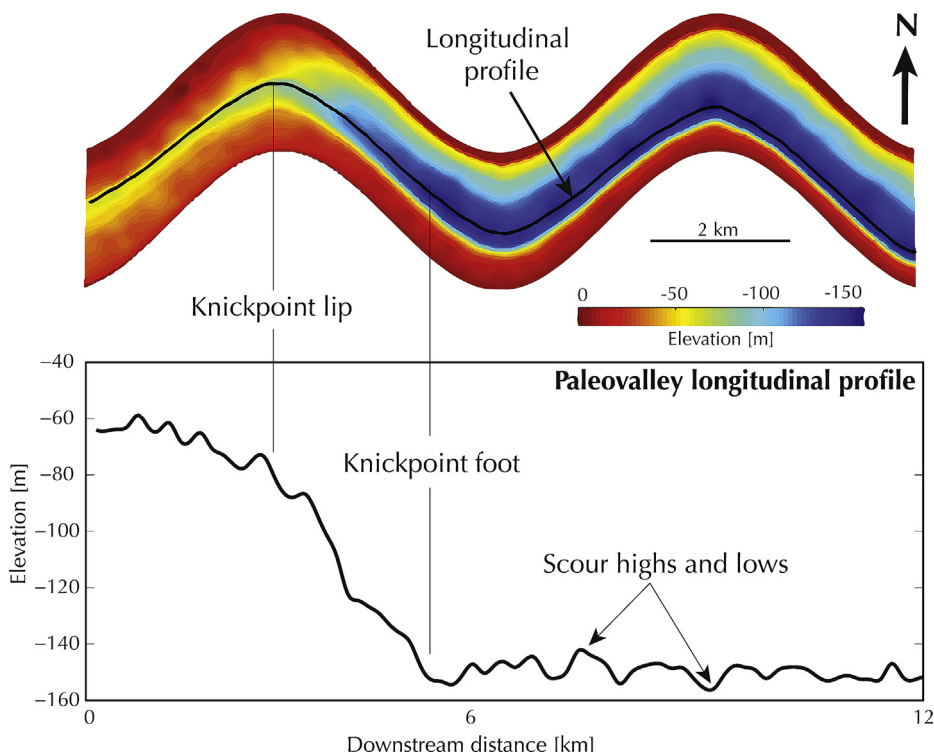


**Fig. 7.** Synthetic test paleovalley surface, including the main features of fluvial bedrock incision including knickpoint and scour features.

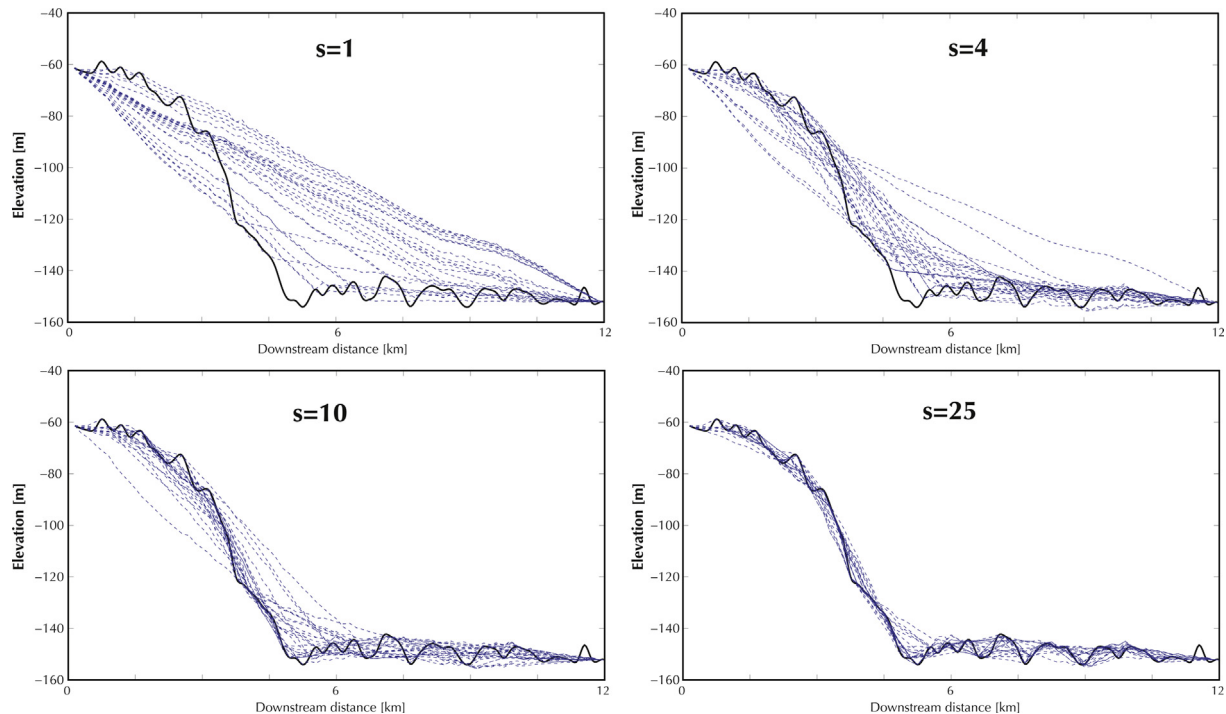


**Fig. 8.** Ensemble longitudinal profiles for four sampling strategies:  $s = 1$ ,  $s = 4$ ,  $s = 10$  and  $s = 12$ . Note the rapid convergence to the reference longitudinal profile for  $s > 4$ .

stationarities such as knickpoints can make it challenging to estimate this aquifer volume. The ensemble volumes for a range of sampling densities are shown in Fig. 10. For sparse sampling, the ensembles present a strong bias to underestimate the volume, however this bias mostly disappears after  $s = 5$ . The real aquifer volume is captured in some cases by even the sparser sampling densities, but this may not correspond to the real longitudinal profile. Therefore, pinpointing possible knickpoints in the paleovalley with the help of prior geological knowledge, can potentially allow accurate estimations of volume with only a few surveys. In

fact, the four realizations labeled with #50 in Fig. 9 have approximately the same volume, as they plot close to the red dashed line in Fig. 10. The ensemble ranges of Fig. 10 also help understanding the reduction of statistical uncertainty that occurs with conducting new surveys or drilling new wells. This figure may serve as an illustration of uncertainty reduction with further surveying. For example, for the given case (based on Fig. 10), it can be argued that future prospecting should lie in the range  $s = 5–15$ , because it removes the underestimation bias whereas further sampling beyond  $s = 15$  yields little gains in terms of reducing uncertainty.

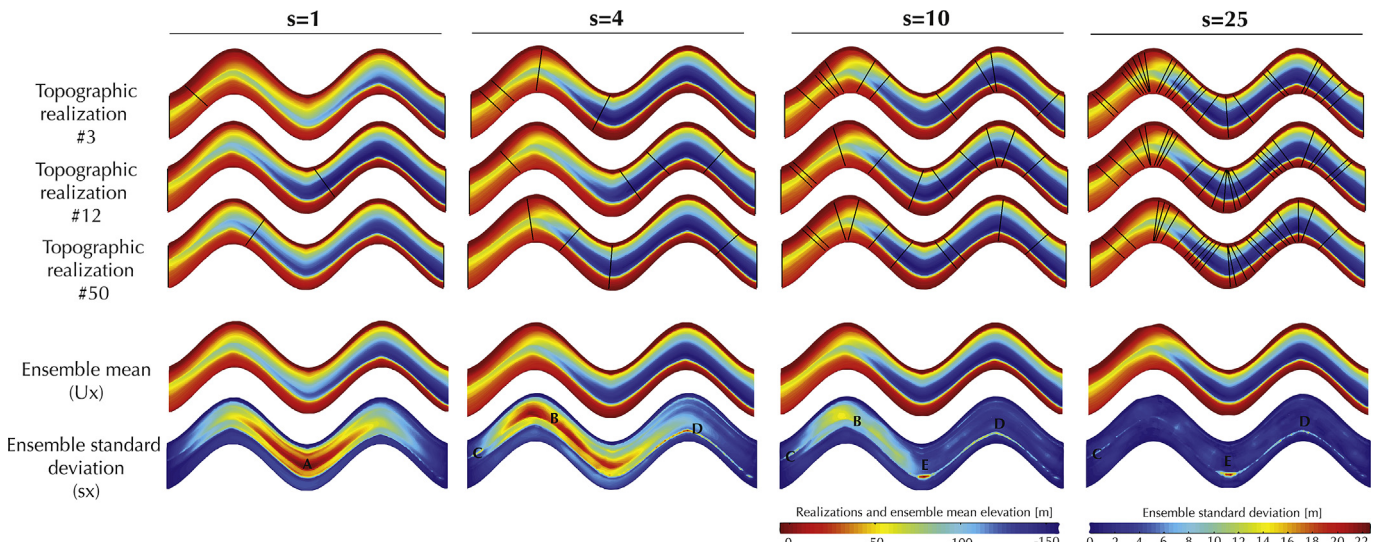


**Fig. 9.** Three sample realizations and ensemble statistics for the characterization of large-scale topographic uncertainties. Columns depict different sampling densities including sparse ( $s = 1$ ), intermediate ( $s = 4, 10$ ) and dense ( $s = 25$ ). The bottom part of the figure shows the ensemble mean and standard deviation for each sampling ensemble, consisting of fifty realizations.

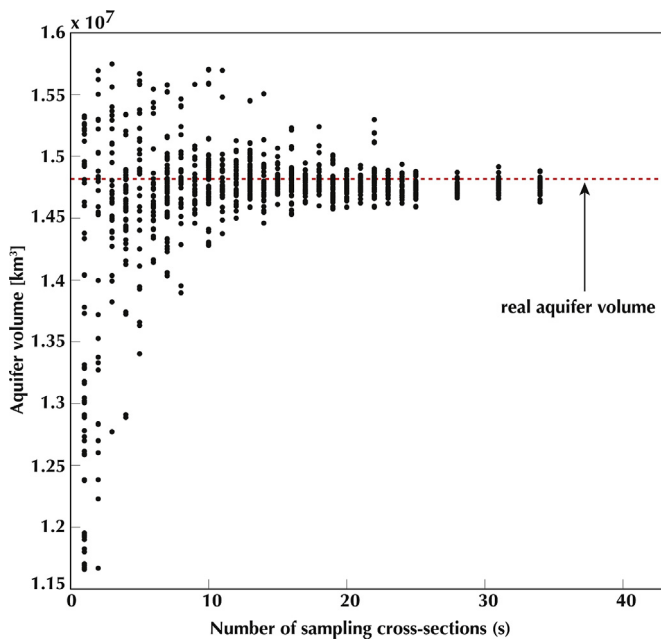


**Fig. 10.** Ensemble aquifer volume estimation for different sampling densities. The red dashed line represents the volume of the reference surface of Fig. 7. (For interpretation of the references to color in this figure legend, the reader is referred to the web version of this article.)

#### 4. Application to the San Jose River aquifer paleovalley

##### 4.1. Study area and input data

The applied case study area is the San Jose River aquifer, a 110 km long fluvial system draining the Azapa valley in Northern Chile (Fig. 11). The coastal area on Northern Chile ( $18^{\circ}\text{S}$ – $30^{\circ}\text{S}$ ) is part of the Atacama Desert, recognized as the driest in the world (Houston and Hartley, 2003; Schulz et al., 2012). The Azapa valley is characterized by extreme aridity, with annual rainfall less than 1 mm in most of the basin (Clarke, 2006). Other localities in this region, such as Iquique and Antofagasta have mean annual rainfall below 0.6 mm (Houston and Hartley, 2003) and certain rainfall monitoring stations have never recorded rainfall. For this reason, groundwater exploitation has been developed in Atacama during the last century to sustain domestic and agricultural activities particularly in the Azapa valley. Groundwater abstractions from this aquifer greatly exceed the long-term sustainable diversion limit. Unfortunately, existing groundwater models that have been developed to predict future conditions of the San Jose River aquifer are based on limited hydrogeological knowledge, and therefore have considerable geological uncertainty. The Azapa valley was formed by the down cutting of the San Jose River in rocks of the Liparitic (Miocene) and Porphyritic (Jurassic-early Cretaceous) Formations. Later in the Pleistocene, the San Jose River began to fill the valley, a process that is ongoing today (Taylor, 1949).

Input datasets for this study consist of  $(x,y,z)$  points in Cartesian coordinates. Pairs  $(x,y)$  correspond to geographical locations according to the UTM WGS84 datum and  $(z)$  is the height above sea level. Elevations are assigned using 3 arc second (30 m resolution) ASTER Global Elevation Data from NASA's Earth Observing System Data and Information System (EOSDIS).

For the San Jose River aquifer several sources of spatial data are available: vertical cross-sections depicting the subsurface boundary between the alluvial fill and the bedrock derived from gravity surveys (Fig. 11b–f); lithological well-logs indicating depth to

bedrock; and the ground surface perimeter of the alluvium, represented by the contact between the alluvium and the bedrock surface (Fig. 11a). Cross-section data for this study was obtained from the public archives of the Chilean General Directorate of Water (DGA). In addition, seven lithological well-logs (Taylor, 1949) depicting depth to bedrock are considered (Fig. 11g). The alluvium/bedrock boundaries were digitized and georeferenced using the open-source GIS package QGIS 1.8 and aerial images.

##### 4.2. Bedrock reconstruction

A total of five geophysical cross-sections were interpolated and integrated with well-log data to create the subsurface paleovalley model for the San Jose River aquifer. The interpolation sequence for the whole basin is presented in Fig. 12a–e. Fig. 12a–d shows the steps leading to the reconstruction of the trend model for this paleovalley. As discussed earlier, the algorithm extracts a channel centerline and then uses it to create a customized grid, defined by a preselected number of interim cross-sections and interpolation nodes. Pairs of geophysical transects are propagated across interim cross-sections, creating a 2D interpolated trend surface (Fig. 12d).

Superimposing correlated topographical noise creates the final paleovalley model. Steps depicted in Fig. 12d,e illustrate the addition of SGS correlated noise to the trend surface, without conditioning to well-log data (an example including conditioning is presented below). The SGS step can be repeated to obtain an ensemble of equally likely bedrock surfaces, reflecting geological uncertainty (one such realization is shown in Fig. 12f).

Considering that the distance between each pair of geophysical cross-sections is on average 10 km, which is challenging for most conventional methods, the final reconstruction of the San Jose River aquifer paleovalley satisfies the main desired features:

- (1) a continuous V-shaped elongated surface,
- (2) connectivity of the longitudinal profile in the downstream direction,
- (3) adequate handling of sinuosity and variable orientations,
- (4) along/across-channel coherence of morphological features,
- (5) conditioning to hard-data,
- (6) a realistic geometry within the limits of the sparse data, and
- (7) the final reconstruction is non-stationary.

For the reconstruction presented in Fig. 12, we employed a total of 700 interim cross-sections and  $7 \times 10^5$  interpolation nodes (1000 per interim cross-section). Considering a total reach of 35 km and average width of 900 m, the paleovalley reconstruction mesh has a resolution of approximately 50 m in the along valley profile and 1 m in the across-valley direction. From a user perspective, the method requires very few parameters and is economical in terms of computation since only linear (or spline) interpolations are performed. The only parameters that are needed correspond to the number of interpolation nodes and interim cross-sections. Although this step can be automated, it provides an opportunity for the practitioner to adjust the model's resolution in terms of the size of the interpolation domain and available CPU resources.

Since the Azapa valley presents a relatively straight path along its profile, in this specific example we make very simple assumptions about the location of the valley bottom. Here, the deepest part of the valley is located by linear interpolation (see Fig. 3d). Although here we do not explicitly introduce a geological analog for the location of the deepest part of the valley, our methodology enforces the general notion that erosion is concentrated on the outside of a bend (Shepherd and Schumm, 1974). This is precisely what is shown in Fig. 12b, between transects T1 and T2. In the remaining parts of the model, the deepest part of the valley is

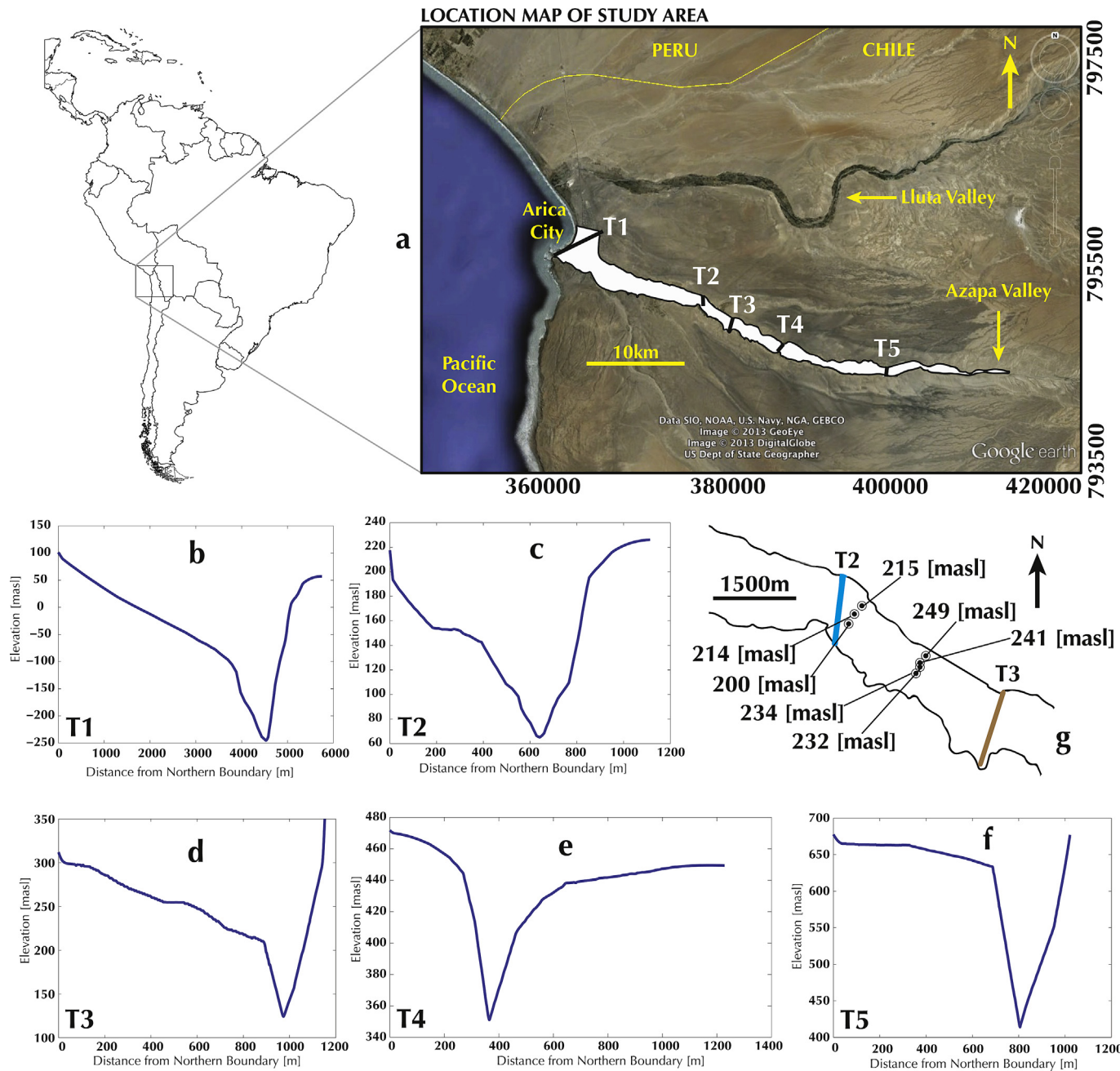


**Fig. 11.** Study area and data in Azapa valley, northern Chile. (a)–(e) Vertical transects of basement depth obtained from Gravimetry studies; (f) Lithological well-log data providing depth to bedrock (Taylor, 1949). Horizontal axes in (a)–(e) represent distance from northern boundary of the paleovalley.

locally constrained by the position indicated on the survey transects. Despite the simple assumption described above, any type of soft geological knowledge can be included. Similarly, variations on the step described in Section 2.1.4 will allow the modeler to 'steer' the valley in a desired direction.

#### 4.3. Characterization of small-scale uncertainties

An important step in this methodology is the selection of an appropriate variogram model to guide the SGS process. This step is aimed at characterizing the small-scale component of topographic uncertainty, such as the erosion signature along the longitudinal profile. In most situations no data are available to infer the basement surface spatial variability, however this can be solved by adopting an analog approach, which we demonstrate below.

To demonstrate the analog approach, we selected an area that characterizes the expected texture of the paleovalley: a  $6.5 \times 2.5$  km polygon of denuded bedrock is chosen and used to infer statistics for a representative model of topographic variability (Fig. 13). This polygon is located at Quebrada Las Lloyas, an outcrop of the Liparitic Formation which forms the bedrock for most of the lower south slopes of the valley (Taylor, 1949). It may be argued that the choice of this particular analog is not optimal, as the surrounding outcropping rock may not convey accurate information about the valley floor variability. We point out that local bedrock outcrops are only one of many possible ways to supplement the paleovalley reconstruction with a geological analog. Other appropriate options for analogs are modern landscapes undergoing comparable erosional processes, outcrops from different locations and results from experimental simulations. Where a modern

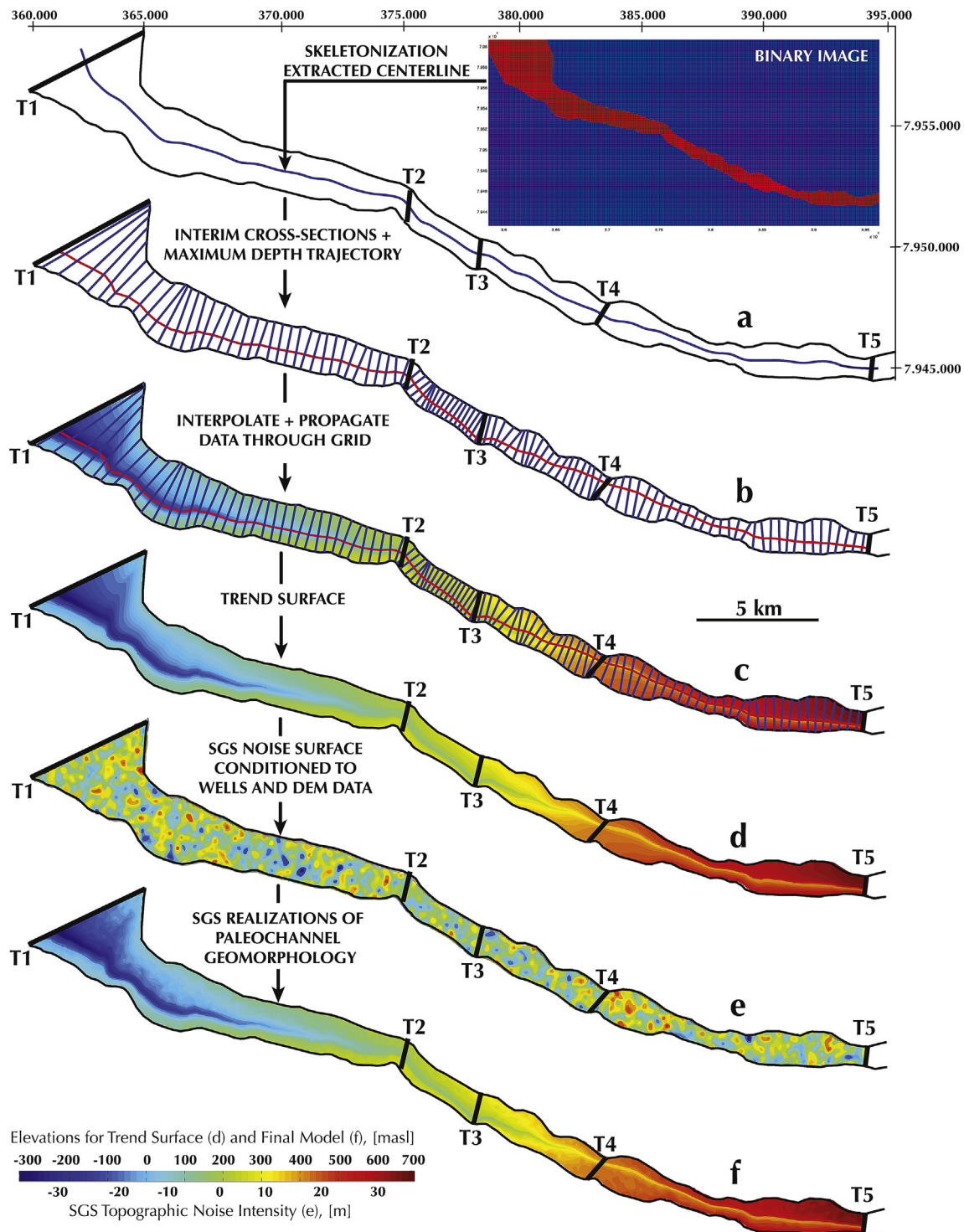


**Fig. 12.** Stepwise reconstruction of the Azapa paleovalley. (a) Extracted centerline using a binary image of the channel and skeletonization; (b) adaptive grid and approximation of the paleovalley bottom; (c)–(d) propagation of geophysical transect data through the grid to obtain a trend surface; (e) generation of a SGS noise surface conditioned to the DEM elevations, well-log data and local topographic variability; (f) final model of the Azapa valley after superimposing trend + SGS surfaces.

analog is not available, geologists may derive synthetic variograms based on their conceptual understanding of the system. Refer to Alexander (1993) for a detailed discussion about the appropriate selection and implementation of geological analogs.

We borrow the variogram characteristics of the analog and impose them on the bedrock surface predictions. Variograms allow conferring a realistic variability valley profile, resembling the

typical morphological characteristics of bedrock incision (e.g. irregularly-spaced scour lows), as shown in Fig. 5m. Within the selected sampling site, we extracted the DEM elevations (Fig. 13a), then estimated a topographic trend using a moving average algorithm (Fig. 13b), and finally subtract the trend from the DEM elevations to obtain a residual surface (Fig. 13c). The moving average procedure allows separating the large-scale geological trend from

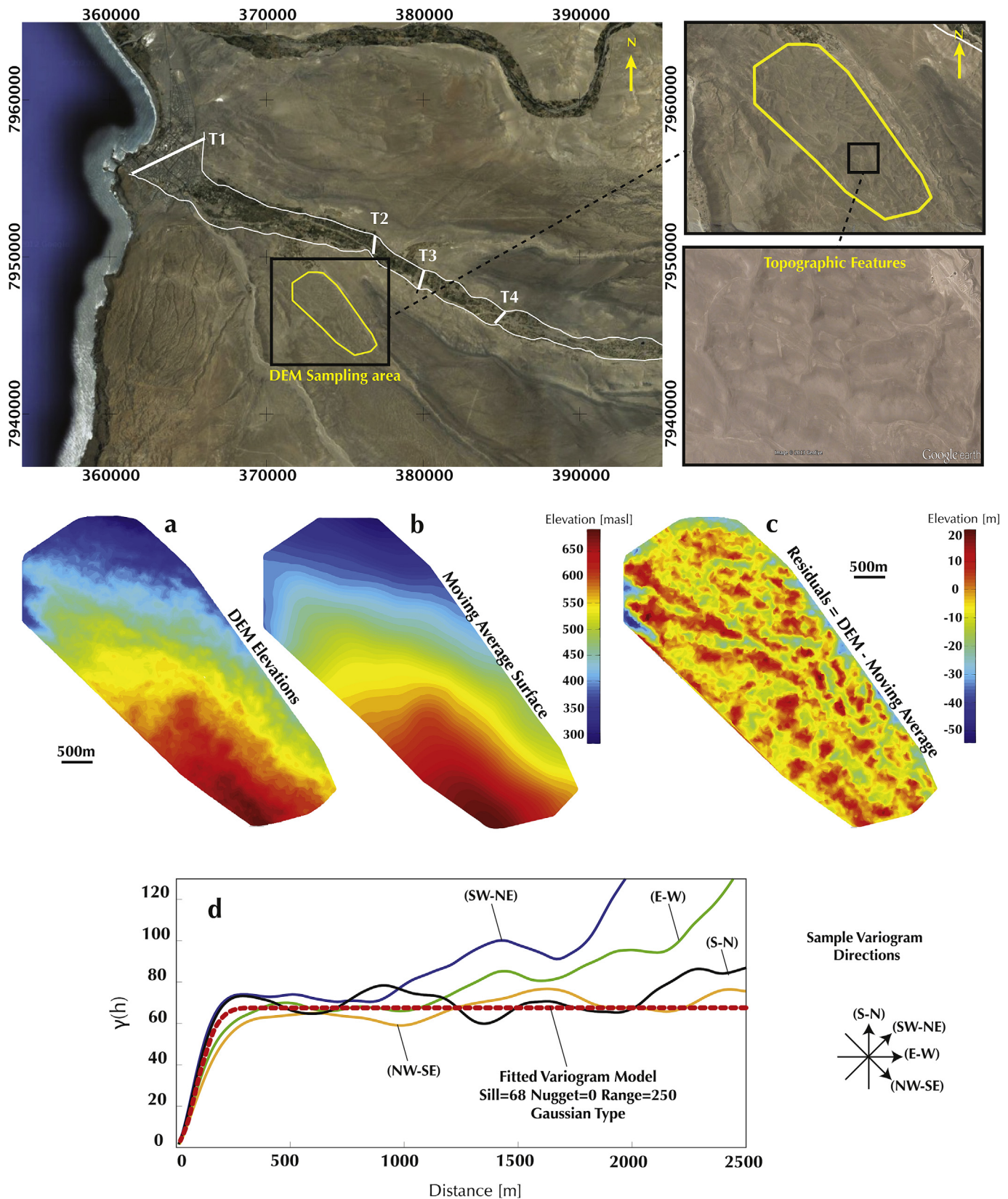


**Fig. 13.** Illustration of using a surface sampling area to capture topographic variability at the study site. (a) DEM elevations; (b) resulting surface after applying a moving average smoothing filter; (c) residual surface; (d) directional variograms of residual surface.

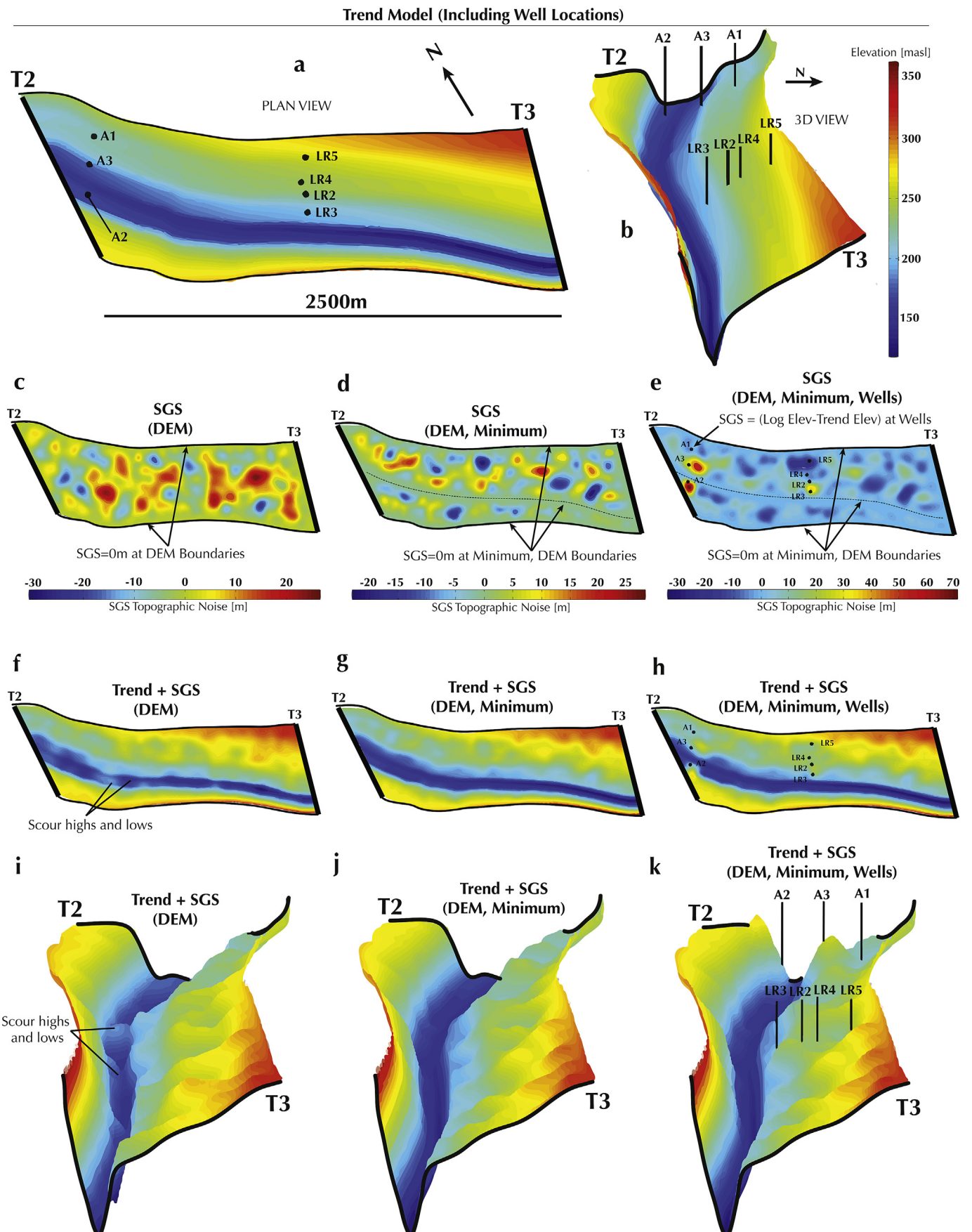


**Fig. 14.** Visual comparison of the interpolation process conditioned with different levels of conditioning to hard data, between transects T2 and T3. (a) Plan view of trend surface and well locations; (b) 3D view of trend surface and well locations. First column is for conditioning only to DEM elevations at the aquifer boundaries, (c)–(f)–(i). Second column shows conditioning for DEM elevations and paleovalley bottom (d)–(g)–(j). Third column adds conditioning to wells data (e)–(h)–(k).

the small-scale spatial variability. This surface represents the roughness and texture that we would like the models to convey. The residual surface is inspected in several orientations, by calculating experimental variograms along four directions, as shown in Fig. 13d. Although there is evidence of weak anisotropy, we have decided to assume isotropy because we only aim at representing small-scale spatial variability. For sparse datasets with large conceptual uncertainty, and difficulty in choosing analogs, finely modeling this slight anisotropy would mean overparameterizing our model, therefore a single Gaussian structure is fitted to the data ( $\text{Sill} = 68$ ,  $\text{Nugget} = 0$ ,  $\text{Range} = 250$ ). Although employing a single variogram across the whole paleovalley carries an assumption about stationarity, this is compensated by the fact that trend surfaces created prior to this step are non-stationary and hence the final models will maintain this characteristic. In the presence of zonal variability, a number of variograms could be derived and applied along different reaches of the valley.

The SGS step also includes conditioning to hard geologic data, a step that introduces flexibility and additional modeling capabilities to the reconstruction process. Fig. 14 presents the superposition of correlated SGS noise conditioned to bedrock depth information extracted from lithological well-log data in an area between geophysical transects T2 and T3 (Fig. 14a,b). Two north-south geological cross-sections have been inferred from wells drilled for crop irrigation in the Azapa valley (Taylor, 1949), showing the Liparitic bedrock surface under the Pleistocene and recent alluvial fill. Table 1 summarizes the available conditioning data from these wells, elevations to the bedrock contact interface and the departure of the actual depths from the trend surface. It should be noted that the SGS implementation requires conditioning data to be expressed as trend departures and not absolute elevations above sea level. These lithological well-logs offer more precise, but discrete (and sparse) information of the bedrock surface, when compared to geophysical data that tends to be continuous. Integrating the two data sources occurs when the trend surface, derived using geophysical surveys, is adjusted to the well-log data using conditional SGS. Special care needs to be taken here, as geophysics is often tied to well-log data for calibration and guiding of the inversion processes. To avoid redundancies, well-log data used for the SGS step needs to be independent of the geophysical data. We took this into consideration for the Azapa valley reconstruction.

Fig. 14a,b shows two views of the trend surface obtained from geophysical transects, and the location of conditioning wells. Fig. 14c–e presents the trend departure surfaces created using SGS. Fig. 14c is conditioned to the DEM only whereas Fig. 14d is conditioned to the DEM and the valley bottom. Fig. 14d demonstrates how the incision signature can be controlled by constraining the trend departure surface along the deepest portion of the paleovalley. The small-scale variability surfaces shown in Fig. 14c–e are adequate for a fluvial valley undergoing a filling process, because they convey the characteristic longitudinal profile scour pattern of these systems. Fig. 14e further adds conditioning to well-log data. It is important to note how the SGS variability surface of Fig. 14e honors the conditioning data given in Table 1. Very little variability needs to be introduced in some locations (wells LR4, LR5 and A1), indicating that the trend model is capable of capturing here the real depth to bedrock. In other locations, such as wells A2, A3 and LR3 this correspondence is not equally satisfactory and the SGS surface presents larger departures. Fig. 14f–h presents the superposition of the previous SGS perturbation surfaces to the trend model of Fig. 14a. These figures illustrate the effects that different combinations of geological data and prior knowledge have on the final paleovalley. Fig. 14i–k presents a 3D view of the resulting geomodels.

**Table 1**

Well-log data available for conditioning the SGS surface. Conditioning elevations are computed as the difference between the lithological well-log and trend at the location. Well notations have been maintained from (Taylor, 1949).

Well	Basement elevation from well log [m] (1)	Basement elevation from trend surface [m] (2)	Conditioning elevation for SGS surface [m] (1) – (2)
LR4	241	260	-19
LR1	234	239	-5
LR2	234	232	2
LR3	232	264	32
A2	200	165	35
A3	214	182	32
A1	215	217	-2

## 5. Discussion and conclusions

In this study we have introduced a stochastic, data-driven workflow for constructing paleovalley bedrock surfaces by integrating geophysical, DEM and lithological well-log data with soft geological knowledge. The technique was validated on a synthetic sine wave channel, and then applied to an alluvial aquifer in the Azapa valley in Northern Chile. Geophysical transects, although often far apart, contain valuable information about the bedrock depth and non-stationarity, which can be translated to a general trend model of the paleovalley. Lithological well-log data provide discrete but accurate bedrock depths, hence it is more suitable for informing the local topography and for guiding a stochastic conditioning process, such as SGS. Finally, DEM raster images can be used to infer small-scale bedrock variability and to integrate the final model with the surrounding topography. This study illustrates that the inclusion of conceptual geological knowledge in the workflow improves how we combine sparse data at multiple scales and resolution. Although subjective and conceptual, geological analogs convey important information about erosional processes that shaped the landscape. This information would be difficult to capture from an individual lithological well-log, the DEM, or geophysical data.

In contrast to hard data, soft knowledge often comes in a more abstract form, as general concepts about sediment transport, geomorphology and erosion. These represent the type of information that is commonly available to guide the construction of geological surfaces. The differing nature of each data source and their intrinsic limitations pose a challenging and ubiquitous problem for hydrogeologists using existing interpolation tools. To solve these issues, we have developed and tested a methodology that adapts and combines established methods from previous research in river bathymetry modeling, structural geology, geostatistics and mathematical morphology. Our approach extends previous work in the field by automating the channel centerline extraction and the subsequent generation of a customized interpolated domain. Additionally, implementing the concept of node pairing enforces the continuity and connectivity of valley shaped structures, which can be challenging for conventional interpolation methods. This approach has important effects on the modeling workflow, since it allows storing, manipulating and integrating the different datasets using ordinary matrices and very simple interpolation methods.

Multi-realization methods have a proven track record in the characterization of geological uncertainty (Refsgaard et al., 2012; Troldborg et al., 2007). Our implementation highlights the value of this approach for the specific problem of predicting the geometry of the alluvium/bedrock interfaces. These simulation-type workflows have been strongly advocated in recent work on structural model uncertainty, as they sample a greater subset of the plausible space of geological models (Bond et al., 2007; Bredehoeft, 2005;

Neuman, 2004; Poeter, 2007; Rojas et al., 2010; Zeng et al., 2013). The result is capturing a greater portion of the uncertainty associated with our limited geological understanding of the system. Overall, the uncertainty characterization exercise presented in this paper shows that a methodology of this kind is likely to capture the large-scale and small-scale morphological uncertainty of fluvial incision into bedrock at a relatively low cost. For the specific case of the Azapa valley, our data suggests that with the current sampling density ( $s = 4$ ) the total aquifer volume is most likely underestimated. Taking the information of Fig. 10 as a reference, we recommend additional prospecting up to  $s = 10–15$ , preferentially at narrow portions of the valley and meanders, where the main non-stationarities of paleovalleys are likely to be located (Gardner, 1983; Phillips and Lutz, 2008; Seidl and Dietrich, 1993; Shepherd and Schumm, 1974; Stock and Montgomery, 1999; Whittaker et al., 2007). This increases the chances of capturing the main features of the paleovalley, and also represents a balance between the cost of future surveys and the need to reduce topographic uncertainty.

Uncertainty in the geophysical transects and lithological well-log data can be addressed in the same multi-realization framework. For instance, several trend surfaces based on alternative inversion models for the geophysical data can be combined with many variable surfaces generated by SGS realizations. In doing so, it is possible to obtain an ensemble of realizations with a wider range of variability, accounting also for the measurement uncertainty.

In summary, our work highlights the value of soft geological knowledge when hard data is limited, and how this knowledge can be integrated and uncertainty characterized using an original workflow. Although our methodology attempts to get a better handle on uncertainties introduced by the lack and different nature of geological data, there is simply no substitute for a good dataset. Despite this methodology being specific to basic valley-shaped structures, the general workflow has the potential to be adapted to more complex geological surfaces. The approach presented here is customizable and general in scope; hence we anticipate applicability to a broad range of valley-shaped morphologies in glacial valleys, river valleys or ocean trenches. The Matlab implementation of this algorithm can be accessed through the supplementary files attached to the electronic version of this article. Future work will focus on modeling structures of increased complexity that are common in hydrogeological studies, such as networks of converging and superimposed paleovalleys, knickpoints and tributary junctions.

## Acknowledgments

The authors would like to thank and the Chilean General Directorate of Water (DGA) for the datasets employed in this study. Funding for the research was provided by the National Centre for Groundwater Research and Training, supported by the Australian Research Council and the National Water Commission. We would also like to thank Gonzalo Diaz for his invaluable support in the coding and conception of this research.

## References

- Alexander, J., 1993. A discussion on the use of analogues for reservoir geology. In: Geological Society, London, Special Publications, vol. 69, pp. 175–194.
- Allan James, L., 1996. Polynomial and power functions for glacial valley cross-section morphology. *Earth Surf. Process. Landforms* 21, 413–432.
- Anderson, R.S., Molnar, P., Kessler, M.A., 2006. Features of glacial valley profiles simply explained. *J. Geophys. Res.* 111, F01004.
- Bangmei, G., Tao, W., Rong, Z., 2010. Research on Extracting Skeleton Line of Polygon. *IEEE*, pp. 514–517.
- Bertoncello, A., Sun, T., Li, H., Mariethoz, G., Caers, J., 2013. Conditioning surface-based geological models to well and thickness data. *Math. Geosci.*, 1–21.
- Bond, C.E., Gibbs, A.D., Shipton, Z.K., Jones, S., 2007. What do you think this is? Conceptual uncertainty in geoscience interpretation. *Math. Geol.* 17, 4.
- Bredehoeft, J., 2005. The conceptualization model problem—surprise. *Hydrogeol. J.* 13, 37–46.
- Caers, J., Zhang, T., 2004. Multiple-point geostatistics: a quantitative vehicle for integrating geologic analogs into multiple reservoir models. *AAPG Mem.* 80, 383–394.
- Clarke, J.D.A., 2006. Antiquity of aridity in the Chilean Atacama Desert. *Geomorphology* 73, 101–114.
- Dubrule, O., 1993. Introducing more geology in stochastic reservoir modelling. In: Soares, A. (Ed.), Quantitative Geology and Geostatistics, Geostatistics Tróia'92. Springer, Netherlands, pp. 351–369.
- Enge, H.D., Buckley, S.J., Rotevatn, A., Howell, J.A., 2007. From outcrop to reservoir simulation model: workflow and procedures. *Geosphere* 3, 469–490.
- Finnegan, N.J., Roe, G., Montgomery, D.R., Hallet, B., 2005. Controls on the channel width of rivers: implications for modeling fluvial incision of bedrock. *Geology* 33, 229.
- Friedmann, F., Chawathe, A., Larue, D.K., 2003. Assessing uncertainty in channelized reservoirs using experimental designs. *SPE Reserv. Eval. Eng.* 6, 264–274.
- Gardner, T.M., 1983. Experimental study of knickpoint and longitudinal profile evolution in cohesive, homogeneous material. *Geol. Soc. Am. Bull.* 94, 664–672.
- Goff, J.A., Nordfjord, S., 2004. Interpolation of fluvial morphology using channel-oriented coordinate transformation: a case study from the New Jersey Shelf. *Math. Geol.* 36, 643–658.
- Gold, C., Snoeyink, J., 2001. A one-step crust and skeleton extraction algorithm. *Surv. Geophys.* 30, 144–163.
- Gonzalez, R.C., Woods, R.E., Eddins, S.L., 2009. Digital Image Processing Using MATLAB, second ed. Gatesmark Publishing.
- Graf, W.L., 1970. The geomorphology of the glacial valley cross section. *Arctic Alp. Res.* 2, 303–312.
- Grammer, G.M., Harris, P.M.M., Eberli, G.P., 2004. Integration of outcrop and modern analogs in reservoir modeling: overview with examples from the Bahamas.
- Gringarten, E., Mallet, J.-L., Alapetite, J., Leflon, B., 2005. Stochastic modeling of fluvial reservoir: the YACS approach. In: Presented at the SPE Annual Technical Conference and Exhibition, pp. 9–12.
- Guardiano, F.B., Srivastava, R.M., 1993. Multivariate Geostatistics: Beyond Bivariate Moments, pp. 133–144.
- Haldorsen, H.H., Chang, D.M., 1986. Notes on stochastic shales: from outcrop to simulation model. In: Reservoir Characterization, pp. 445–485.
- Hansen, T., 2004. mgstat: a Geostatistical Matlab Toolbox. Online web resource. URL: <http://mgstat.sourceforge.net>.
- Haunert, J.-H., Sester, M., 2007. Area collapse and road centerlines based on straight skeletons. *Math. Geol.* 12, 169–191.
- Houston, J., Hartley, A.J., 2003. The central Andean west-slope rainshadow and its potential contribution to the origin of hyper-aridity in the Atacama Desert. *Int. J. Climatol.* 23, 1453–1464.
- Hoyos, A. de, Viennot, P., Ledoux, E., Matray, J.-M., Rocher, M., Certes, C., 2012. Influence of thermohaline effects on groundwater modelling – application to the Paris sedimentary Basin. *J. Hydrol.* 464–465, 12–26.
- Hu, L.Y., Chugunova, T., 2008. Multiple-point geostatistics for modeling subsurface heterogeneity: a comprehensive review. *Water Resour. Res.* 44, W11413.
- Jaireth, S., Clarke, J., Cross, A., 2010. Exploring for sandstone-hosted uranium deposits in paleovalleys and paleochannels. *Geosci. Aust. Ausgeo News* 97, 1–5.
- Jones, R.R., McCaffrey, K.J., Imber, J., Wightman, R., Smith, S.A., Holdsworth, R.E., Clegg, P., De Paola, N., Healy, D., Wilson, R.W., 2008. Calibration and validation of reservoir models: the importance of high resolution, quantitative outcrop analogues. In: Geological Society, London, Special Publications, vol. 309, pp. 87–98.
- Kirsch, R., 2008. Groundwater Geophysics: A Tool for Hydrogeology, 2nd ed. Springer.
- Le Loc'h, G., Beucher, H., Galli, A., Doligez, B., 1994. Improvement in the truncated Gaussian method: combining several Gaussian functions.
- Legleiter, C.J., Kyriakidis, P.C., 2008. Spatial prediction of river channel topography by kriging. *Earth Surf. Process. Landforms* 33, 841–867.
- Li, J., Heap, A.D., 2011. A review of comparative studies of spatial interpolation methods in environmental sciences: performance and impact factors. *Ecol. Inform.* 6, 228–241.
- Li, Y., Liu, G., Cui, Z., 2001. Glacial valley cross-profile morphology, Tian Shan Mountains, China. *Geomorphology* 38, 153–166.
- Liu, Y., Harding, A., Abriel, W., Strebelle, S., 2004. Multiple-point simulation integrating wells, three-dimensional seismic data, and geology. *AAPG Bull.* 88, 905–921.
- MacGregor, K.R., Anderson, R.S., Anderson, S.P., Waddington, E.D., 2000. Numerical simulations of glacial-valley longitudinal profile evolution. *Geology* 28, 1031–1034.
- Mariethoz, G., Kelly, B.F., 2011. Modeling complex geological structures with elementary training images and transform-invariant distances. *Water Resour. Res.* 47, W07527.
- Mariethoz, G., Renard, P., Cornaton, F., Jaquet, O., 2008. Truncated plurigaussian simulations to characterize aquifer heterogeneity. *Earth Surf. Process. Landforms* 47, 13–24.
- Merwade, V.M., 2009. Effect of spatial trends on interpolation of river bathymetry. *J. Hydrol.* 371, 169–181.

- Merwade, V.M., Cook, A., Coonrod, J., 2008. GIS techniques for creating river terrain models for hydrodynamic modeling and flood inundation mapping. *Environ. Model. Softw.* 23, 1300–1311.
- Merwade, V.M., Maidment, D.R., Goff, J.A., 2006. Anisotropic considerations while interpolating river channel bathymetry. *J. Hydrol.* 331, 731–741.
- Merwade, V.M., Maidment, D.R., Hedges, B.R., 2005. Geospatial representation of river channels. *J. Hydrol. Eng.* 10, 243–251.
- Michael, H.A., Li, H., Boucher, A., Sun, T., Caers, J., Gorelick, S.M., 2010. Combining geologic-process models and geostatistics for conditional simulation of 3-D subsurface heterogeneity. *Water Resour. Res.* 46, W05527.
- Neuman, S.P., 2004. Stochastic groundwater models in practice. *Stoch. Environ. Res. Risk Assess.* 18, 268–270.
- Neuweiler, I., Vogel, H.-J., 2007. Upscaling for unsaturated flow for non-Gaussian heterogeneous porous media. *Water Resour. Res.* 43.
- Niblack, C.W., Gibbons, P.B., Capson, D.W., 1992. Generating skeletons and center-lines from the distance transform. *Comput. Geosci.* 54, 420–437.
- Nordfjord, S., Goff, J.A., Austin, J.A., Sommerfield, C.K., 2005. Seismic geomorphology of buried channel systems on the New Jersey outer shelf: assessing past environmental conditions. *Mar. Geol.* 214, 339–364.
- Phillips, J.D., Lutz, J.D., 2008. Profile convexities in bedrock and alluvial streams. *Geomorphology* 102, 554–566.
- Poeter, E., 2007. All models are wrong, how do we know which are useful? *Ground Water* 45, 390–391.
- Pringle, J.K., Howell, J.A., Hodgetts, D., Westerman, A.R., Hodgson, D.M., 2006. Virtual outcrop models of petroleum reservoir analogues: a review of the current state-of-the-art. *First Break* 24.
- Rathbun, S.L., 1998. Spatial modelling in irregularly shaped regions: kriging estuaries. *Environmetrics* 9, 109–129.
- Refsgaard, J.C., Christensen, S., Sonnenborg, T.O., Seifert, D., Højberg, A.L., Troldborg, L., 2012. Review of strategies for handling geological uncertainty in groundwater flow and transport modeling. *Adv. Water Resour.* 36, 36–50.
- Remy, N., Boucher, A., Jianbing, W.U., 2009. Applied geostatistics with SGeMS: a user's guide. *Lead. Edge* 28.
- Rojas, R., Kahunde, S., Peeters, L., Batelaan, O., Feyen, L., Dassargues, A., 2010. Application of a multimodel approach to account for conceptual model and scenario uncertainties in groundwater modelling. *Comput. Geosci.* 394, 416–435.
- Schulz, N., Boisier, J.P., Aceituno, P., 2012. Climate change along the arid coast of northern Chile. *Int. J. Climatol.* 32, 1803–1814.
- Seidl, M.A., Dietrich, W.E., 1993. The problem of channel erosion into bedrock. *Catena Suppl.* 23, 101.
- Serra, J.P., Soille, P., 1994. *Mathematical Morphology and its Applications to Image Processing*. Kluwer Academic Pub.
- Shepherd, R.G., Schumm, S.A., 1974. Experimental study of river incision. *Geol. Soc. Am. Bull.* 85, 257–268.
- Sklar, E., 2007. NetLogo, a multi-agent simulation environment. *Artif. Life* 13, 303–311.
- Stock, J.D., Montgomery, D.R., 1999. Geologic constraints on bedrock river incision using the stream power law. *J. Geophys. Res.* 104, 4983.
- Taylor, G.C., 1949. Geology and ground water of the Azapa valley, Province of Tarapaca, Chile. *Econ. Geol. Bull.* 44, 40–62.
- Troldborg, L., Refsgaard, J.C., Jensen, K.H., Engesgaard, P., 2007. The importance of alternative conceptual models for simulation of concentrations in a multi-aquifer system. *Hydrogeol. J.* 15, 843–860.
- Tye, R.S., 2004. Geomorphology: an approach to determining subsurface reservoir dimensions. *AAPG Bull.* 88, 1123–1147.
- Whiteley, R.J., 2005. Gravity mapping and seismic imaging of paleochannels on large tunnel routes in Sydney, Australia. *Geotechn. Eng. Geophys.* 2, 549–558.
- Whittaker, A.C., Cowie, P.A., Attal, M., Tucker, G.E., Roberts, G.P., 2007. Bedrock channel adjustment to tectonic forcing: Implications for predicting river incision rates. *Geology* 35, 103.
- Zeng, X., Wang, D., Wu, J., 2013. Reliability analysis of the groundwater conceptual model. *Hum. Ecol. Risk Assess. Int. J.* 19, 515–525.
- Zinn, B., Harvey, C.F., 2003. When good statistical models of aquifer heterogeneity go bad: a comparison of flow, dispersion, and mass transfer in connected and multivariate Gaussian hydraulic conductivity fields. *Water Resour. Res.* 39, WR001146.